Modelling primary production in the North Sea: Applying a light-dependent model on MERIS images between 2002-2012

Robyn Gwee Simin (5947901)

r.robyngweesimin@students.uu.nl

30 ECTS

Supervisors:

Steven de Jong – Utrecht University   *s.m.dejong@uu.nl*

Jack Middelburg – Utrecht University   *j.b.m.middelburg@uu.nl*

Daphne van der Wal – NIOZ (Yerseke)   *Daphne.van.der.Wal@nioz.nl*

Jacco Kromkamp – NIOZ (Yerseke)   *Jacco.Kromkamp@nioz.nl*

NIOZ Royal Netherlands Institute for Sea Research

Universiteit Utrecht

Faculty of Geosciences

Table of Contents

Table of Figures

Abstract

Primary production in coastal waters is important to monitor due to its implications on water quality, fish stocks and the carbon cycle, amongst others. Due to the economic and political importance of the North Sea, long-term monitoring primary production in this region is essential to fully assess the role of climate change on this process. To apply this to the North Sea, a simple light-dependent primary production model by Cole & Cloern was applied onto in-situ data of water quality parameters and regressed against gross primary production values from OS9, a station off the coast of the Eastern Scheldt. Following calibration at this station and validation of water quality parameters at Rijkswaterstaat stations for the Dutch North Sea, primary production was then successfully modelled for the entire North Sea between 2002-2011 using satellite-derived estimates of water quality parameters (K_d and chlorophyll-a) from Envisat MERIS and surface irradiance (E_o) from a NOAA atmospheric model. Results showed that the various hydrodynamic regions had different primary production values and also experienced variable fluctuations in primary production over the years. It was also found that small changes in the largest hydrodynamic regions had the greatest influence on the North Sea primary production budget. No significant trend was found in the annual primary production budget of the North Sea over the period 2003-2011 (p-value =0.595). The results also showed that modelled primary production values were able to detect shifts in trends as a result of climatic variability, although the period of analysis was quite short to properly assess significant long-terms shifts in primary production trends. Finally, the non-linear response of each region to climatic changes was evident in the annual primary production budget, especially in the case of 2010. A proposed method of conducting future analyses on primary production trends is assessing periods in the North Sea separated by regime shifts to understand the effects of environmental change on phytoplankton population shifts and the effects on primary production.

1 Introduction

The North Sea is a semi-enclosed sea located on the Northwest European continental shelf with an average depth of 90m and an approximate area of 750,000km² (Paramor et al., 2009). The boundary limits are defined by the International Hydrographic Organization and are illustrated in Figure 1. The North Sea remains an important marine traffic route, with one of the busiest shipping lanes in the world (Walker et al., 2016). The Norwegian Trough is the deepest part of the region, with depths of up to 700m (Ducrotoy et al., 2000). The overall bathymetry of the North Sea is also illustrated in Figure 2. Most of the North Sea coasts consists of estuaries and shallow sedimentary features i.e. tidal flats, that provide optimal conditions for a highly productive system, and hence, supporting the fisheries in the region (Ducrotoy & Elliot, 2008). Additionally, the North Sea is a basin that generates a high source of income from several activities such as hydrocarbons extraction, fishing, renewable energy etc. (Ministry of Infrastructure and Environment & Ministry of Economic Affairs, 2015), with income from fishing in the North Sea bringing in €1.6 billion alone in 2014 (STECF, 2016). Considering the ecological functions and socio-economic significance of the

Figure 1: Map of the North Sea region as defined by the International Hydrographic Organization

North Sea, it is therefore an important region to monitor and conserve. Primary production is a process defined as the fixing of inorganic carbon into available energy in the form of organic carbon and is most commonly achieved through photosynthesis. Photosynthesis involves converting carbon dioxide into glucose by using light as a source of energy and therefore, primary production is expressed as the total amount of depth-integrated carbon fixed per area per unit of time, or $gC/m^2/t$ (t = time). Many factors can influence primary production, such as light and nutrient availability, growth rate, physical water characteristics, grazing intensity etc., although the governing factors are mainly temperate, light, nutrient limitations (Field et al., 1998). The common terms found in literature that describe primary production are *net primary production* (NPP) and *gross primary production* (GPP). GPP refers to the total amount of carbon fixed in a given period, while NPP refers to the amount of production that occurs after accounting for the energy used in respiration by the autotrophs. Primary production is important due to its influence on the carbon cycle (Falkowski et al., 1998), estimation of fishing yields (Houde & Rutherford, 1993) and a water quality indicator (Marasovic & Ninceveic, 1997). A model by Holt et al. (2016) predicts that under the business-as-usual climate change scenario, primary production is likely to decrease at mid latitudes and increase at high latitudes. Results from their study show that for the North Sea in particular, there is evidence for a statistically significant decrease in primary production for 76% of the area, especially the coastal regions in the south and southeast i.e. along the Belgian, Dutch and German coasts and near the English Channel. Another study was conducted using in-situ measurements to model primary production, and results showed statistically significant decrease in North Sea primary production between 1988-2013 (Capuzzo et al., 2017). Decreasing primary production would be a great concern for the North Sea, as this mainly governs an ecosystem's ability as a productive fishery (Pauly & Christensen, 1995; Pikitch et al., 2004; Friedland et al., 2012). In addition, changes in primary production may affect the North Sea's role as a sink for organic carbon (Thomas et al., 2005). Many of the proposed causes for changes in long-term primary production have been attributed to climate change (Tiselius et al., 2015; Blanchard et al., 2012; Hays et al., 2005, Capuzzo et al., 2015, Moore et al., 2018), though the exact mechanism driving the change is unclear. Hence, results of decreasing trends in primary production observed in these models allude to a worrying future for the North Sea.

Considering the region's ecological significance and the important functions it provides for the countries surrounding it, primary production is an important parameter to monitor regularly. The most common methods of measuring primary production is through the ^{14}C-labelling method (Pemberton et al., 2006). Other less well-known methods of estimating primary production is through the FRRF (Fast Repetition Rate Fluorometry). Yet, some of the issues surrounding the use of these methods are the cost, and the lack of spatial and temporal resolution across an area. Although the FRRF method can achieve a higher temporal resolution than the ^{14}C method for example (Aardema et al., 2018), it is unable to achieve a synoptic view of the spatial heterogeneity in primary production trends. As primary production has such high spatial and temporal variability, these methods are less suitable for high resolution measurements of long-term trends in primary production. Remote sensing, on the other hand, offers itself as a valuable cost-effective alternative as it is able to capture large-scale patterns of primary production in the North Sea.
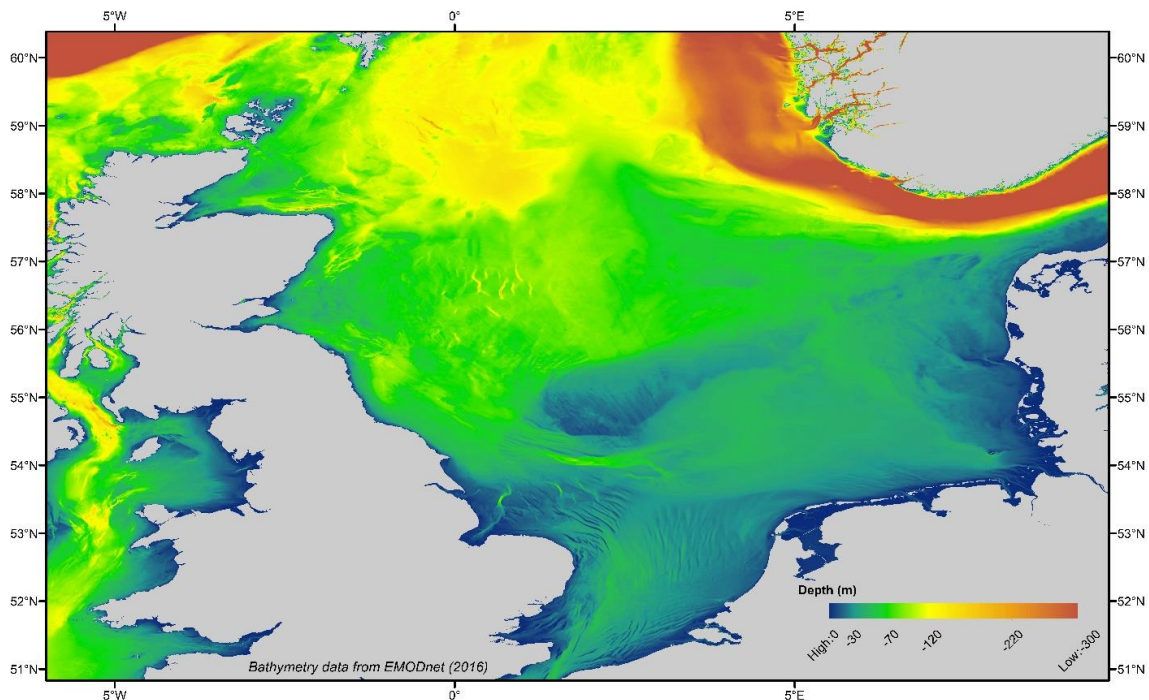
Figure 2: Bathymetry map of the North Sea (data acquired from EMODnet)

In 1978, the Coastal Zone Colour Scanner (CZCS) was launched, which debuted the era of remote sensing of ocean colour from satellites. Aimed at measuring chlorophyll, suspended matter, salinity and temperature, the instrument had a resolution of 800 meters and was operational between 1978-1986 (National Space Science Data Centre, retrieved 13-05-2018). After a hiatus of approximately 10 years, the Sea-viewing Wide Field-of-view Sensor (SeaWiFS) was launched in 1997, followed by the Moderate-resolution Imaging Spectroradiometer (MODIS) and Medium Resolution Imaging Spectrometer (MERIS) (McClain, 2009). What satellite remote sensing of oceans provide that in-situ measurements

of water quality parameters cannot, is achieving a much larger synoptic coverage of spatial trends. Furthermore, ocean colour satellites such as SeaWiFS and MERIS provide complimentary data services, therefore, remote sensing offers itself as a much cheaper method for regular monitoring of important water quality parameters. With the recent launch of Sentinel 3B, a dedicated Earth Observation satellite for oceanographic purposes by the European Space Agency (ESA), developments are still underway to improve the reliability of satellite-derived ocean colour data and increase both spatial and spectral resolution of the images acquired (Ruddick et al., 2008).

In view of the urgent need to maintain a reliable method of regularly monitoring water quality parameters in the North Sea, a pilot project was undertaken in 2017 to test the feasibility of modelling primary production using just three variables which are available as part of the range of MERIS products by applying a light-dependent model onto the Scheldt Estuary in the southwest of The Netherlands. Results showed that primary production could be successfully modelled, with an r^2 of 0.82 for clearer waters, such as the Eastern Scheldt (Gwee, 2017). However, results also showed that there is still a need to improve the accuracy of parameter retrieval for more turbid waters, although this is difficult due to the interference of Coloured Dissolved Organic Matter (CDOM) and Suspended Particulate Matter (SPM) on the image spectra, resulting in some inaccuracies when retrieving water quality parameters from satellite-derived measurements. Another issue was that the area of analysis was much smaller than the North Sea, therefore, it was uncertain if the results of modelling primary production in the Westerschelde was indicative of the performance of the model due to the complex influence of high SPM concentrations on accurately retrieving water quality parameters. As part of the extension of the pilot project to assess the feasibility of applying the same primary production model onto regional seas, the objective of this project is to first model primary production values using in-situ measured water quality parameters from station OS9 (Schouwen) off the coast of the Eastern Scheldt and evaluate the outcome of this process. The model used will be a light-dependent model by Cole & Cloern (1987) and will be calibrated for by linearly regressing against ^{14}C-measured GPP values from OS9 as well. Following which, validation of satellite-retrieved water quality parameters (i.e. chlorophyll-a, Suspended Particulate Matter concentrations, light attenuation coefficient) from the MERIS sensor will be performed by comparing it against in-situ measured datasets obtained from the Rijkswaterstaat. Over- and underestimations are accounted for and correction factors will be applied where appropriate. Finally, gross primary production values will be modelled for the entire North Sea between the years 2002-2012 and the total annual primary production budget of the North Sea will be calculated. Furthermore, primary production will be calculated for each of the six hydrodynamic regions in the North Sea (from van Leeuwen et al., 2015). These regions are significantly different from each other based on density, mixing regime and light climate. The results obtained from this project will hopefully contribute to a growing understanding of

the dynamic nature of the North Sea, and how various drivers of environmental forcing affects primary production on a longer timescale.

2 Materials & Methods

2.1 Model

2.1.1 *BPI*

This project used a light-dependent, semi-empirical model by Cole & Cloern (1987), which has also been successfully applied in the Westerschelde (Scheldt Estuary, The Netherlands by Kromkamp & Peene, 2005). The model describes primary production as a function of phytoplankton biomass (*B*), photic depth *P* and surface downwelling irradiance (*I*). Thus, the product of these terms would then be regressed against in-situ measured primary production values to derive the semi-empirical relationship between primary production and the product of the various parameters. The equation is described below in Equation 1. The parameters are also described in further detail in Table 1.

Equation 1

$$BPI = \text{chl-a} * Z_{eu} * E_o$$

Equation 2

$$BPI = \text{chl-a} * \left(\frac{4.6}{K_d} \right) * E_o$$

Table 1: Description of parameters in the BPI model

Parameters		Units
Abbreviation	Description	
Chl-a	Chlorophyll-a	mg/m^3
Z_{eu}	Photic depth	m^{-1}
E_o	Downwelling surface irradiance	E/m^2/day
K_d	Light attenuation coefficient	m^{-1}

Photic depth Z_{eu} refers to the depth at which photosynthetically available radiance, typically between 400-700nm, falls to 1% below the surface of the water. As it can also be represented as a function of light attenuation coefficient, the photic depth parameter in Equation 1 is therefore replaced by $\frac{4.6}{K_d}$, where K_d represents the light attenuation coefficient. The value *4.6* derived due to the mathematical relationship between light attenuation and euphotic depth (depth at which light attenuates to 1%), which is as follows:

$$100e^{-K_d * Z_{eu}} = 1$$

$$e^{-K_d * Z_{eu}} = 0.01$$

$$Z_{eu} = \ln(0.01) / K_d$$

Therefore, $Z_{eu} = 4.6/K_d$

This is used with two assumptions in mind - that the water column is not stratified and that, therefore, light attenuates constantly with depth (Kirk, 2011). These assumptions may not necessarily hold true for the application of the model onto the North Sea due to the variety of water types in the region, therefore, this must be kept in mind.

The light-dependent model of Cole & Cloern is most suitable for nutrient-rich water environments that are limited by light (Heip et al., 1995). The dynamic nature of the North Sea through space and time may mean that light limitation is not always present throughout, but since the project aims to test the validity of using a simple model to derive estimates of primary production for a much larger region, the results are derived with this assumption in mind. First, the BPI composite parameter is calculated by multiplying the three parameters as shown in Equation 2, including accounting for light attenuation as a function of photic depth. Following which, the composite parameter is regressed against in-situ measured primary production values, which in this project, will use gross primary production (GPP) values derived from 2-hr incubation periods and labelled using the ^{14}C-method. Primary production is, therefore, modelled by deriving a semi-empirical relationship between calculated BPI values and measured GPP values. The GPP values are taken from OS9, a station off the coast of southwest Netherlands. The linear relationship between the BPI composite parameter and measured in-situ primary production values gives rise to the a (slope) and b (correction factor) terms, and the entire model is therefore summarised in Equation 3 below. The linearity of this function could not be tested in this project due to the small number of samples available from station OS9.

Equation 3

$$Primary\ production = a\left[chl\text{-}a * \left(4.6/K_d\right) * E_o\right] + b$$

To apply this model onto satellite-derived images of the North Sea, water quality parameters must first be validated for the North Sea. For this, not only were the parameters directly used in Equation 3 considered, Suspended Particulate Matter (SPM) was also validated as this parameter has been shown to be highly correlated with K_d. Chlorophyll-a, light attenuation coefficient and SPM of the Dutch part of the North Sea are provided by the Rijkswaterstaat for 20 stations. These stations are illustrated in Figure 4 in red triangles. Satellite images with dates coinciding with the dates of the measured values by the

Rijkswaterstaat were downloaded and the three water quality parameters were retrieved and subsequently compared against measured values. Over- or underestimations were accounted for through the validation and, if necessary, correction factors were applied onto the satellite-derived estimates of the water quality parameters before applying the model onto the satellite images. After validation and correction of satellite-derived images, the BPI composite parameter for satellite images was calculated by multiplying the images together, and the *a* and *b* terms derived from the regression of the OS9 derived BPI composite parameter and measured GPP values were applied onto MERIS images of the North Sea between 2002-2012. The process of applying the model onto satellite images is outlined in Figure 3. In addition, primary production values were calculated for each individual hydrodynamic region within the North Sea. Based on van Leeuwen et al. (2015), there are 6 hydrodynamic regions within the North Sea, classified based on the density and stratification regime. The regions are: Seasonally stratified, permanently mixed, permanently stratified, region of freshwater influence, transitional region and intermittently stratified (Figure 4).
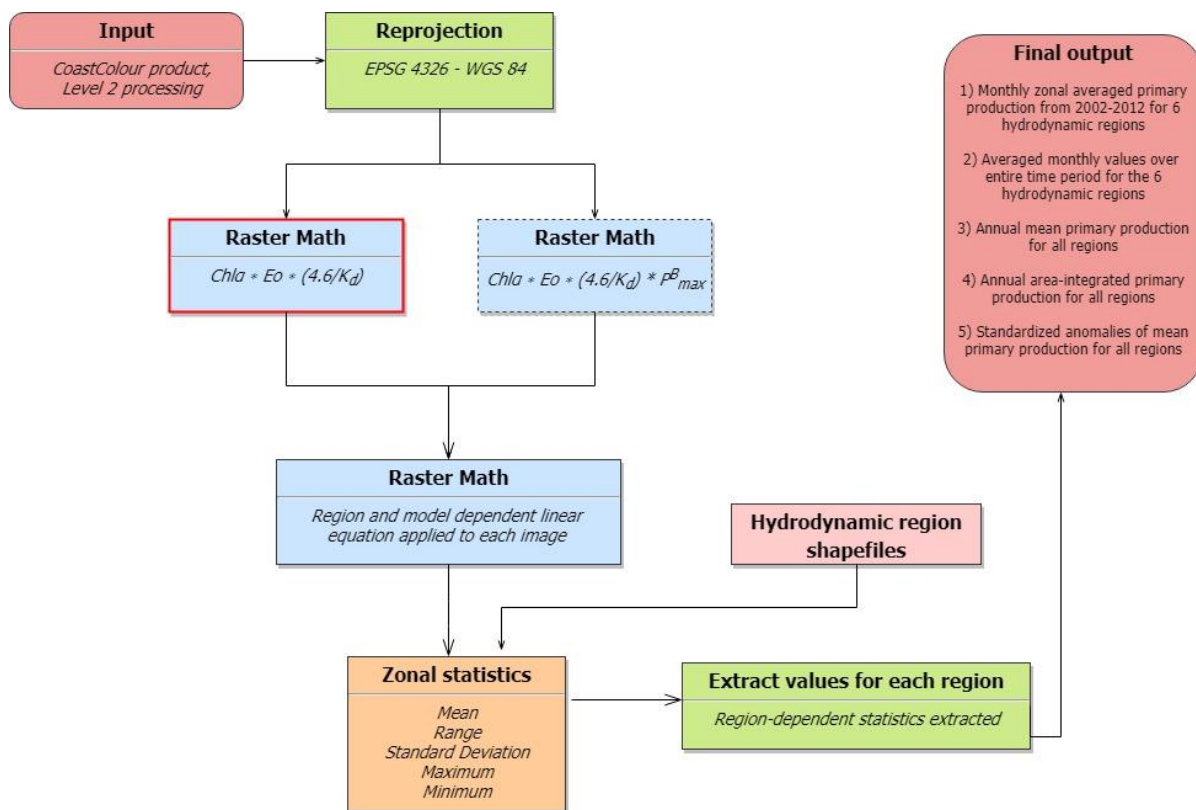
Figure 3: Flow chart of modelling process. The highlighted 'Raster Math' process was the only one used in this project as inclusion of the P_{max} parameter to constrain results was not possible due to insufficient in-situ values.

2.1.2 P^b_{max}

The BPI model is a light-dependent model that includes biomass, however, it does not consider the maximum rate of photosynthesis that can occur in a water column (P^b_{max}). P^b_{max} refers to the maximum rate of photosynthesis per mg of chlorophyll-a in a water column at a certain irradiance (Behrenfeld & Falkowski, 1997). This parameter can be added to the BPI model by including P^b_{max} as a function of primary production. In the pilot study of the Scheldt (Gwee, 2017), the accuracy of modelling primary production based on in-situ data improved by 30% when P^b_{max} was included in the BPI model. Yet, when the model was later applied onto satellite imagery, the r^2 values derived from comparing measured and modelled primary production values showed that the simple BPI model alone performed significantly better than the BPI model with P^b_{max} incorporated (0.82 vs 0.6 respectively in Gwee, 2017). As the Scheldt is only a small area, this parameter was still tested in this project for suitability in a much bigger regional context. Using measured P^b_{max} values from OS9, suitability was tested by deriving a BPI*P^b_{max} composite parameter and regressing against measured GPP values. The summary of the model with the inclusion of this parameter is shown in Equation 4.

Equation 4

$$Primary\ production\ =\ a\left[chl\text{-}a * \left(\frac{4.6}{K_d}\right) * E_o * P^b_{max}\right] + b$$

2.2 In-situ datasets
2.2.1 *Station OS9*

Several in-situ derived water quality parameters were used for validation purposes and calibration of model prior to use on satellite images. The datasets are provided by NIOZ (Kromkamp, unpublished) and the specific station used is from OS9 (Schouwen 4) off the coast of the South-west Netherlands, with the coordinates 51° 40' 47.532", 3° 33' 45.792". The location of OS9 is represented by a circle in Figure 4. Water quality parameters used for this study include suspended particulate matter (SPM) concentrations, chlorophyll-a, gross primary production (GPP), light attenuation coefficient (K_d) and surface irradiance (E_o). GPP was measured based on the uptake of radioactive $^{14}CO_2$ during 2-hr incubations at a range of light intensities, and the methodology is described in detail for all parameters in Kromkamp et al. (1995) and Kromkamp & Peene (2005).

2.2.2 *Rijkswaterstaat stations*

In-situ measured datasets of chlorophyll-a, suspended particulate matter and light attenuation coefficient were downloaded from the Rijkswaterstaat database (https://www.informatiehuismarien.nl/), and the standard protocol and methodology for measurement of each parameter is available via the Rijkswaterstaat website. Data were taken from 20 stations between 2002-2012 that were off the coast of the Netherlands and the locations of the stations are illustrated in Figure 4 (red triangles).
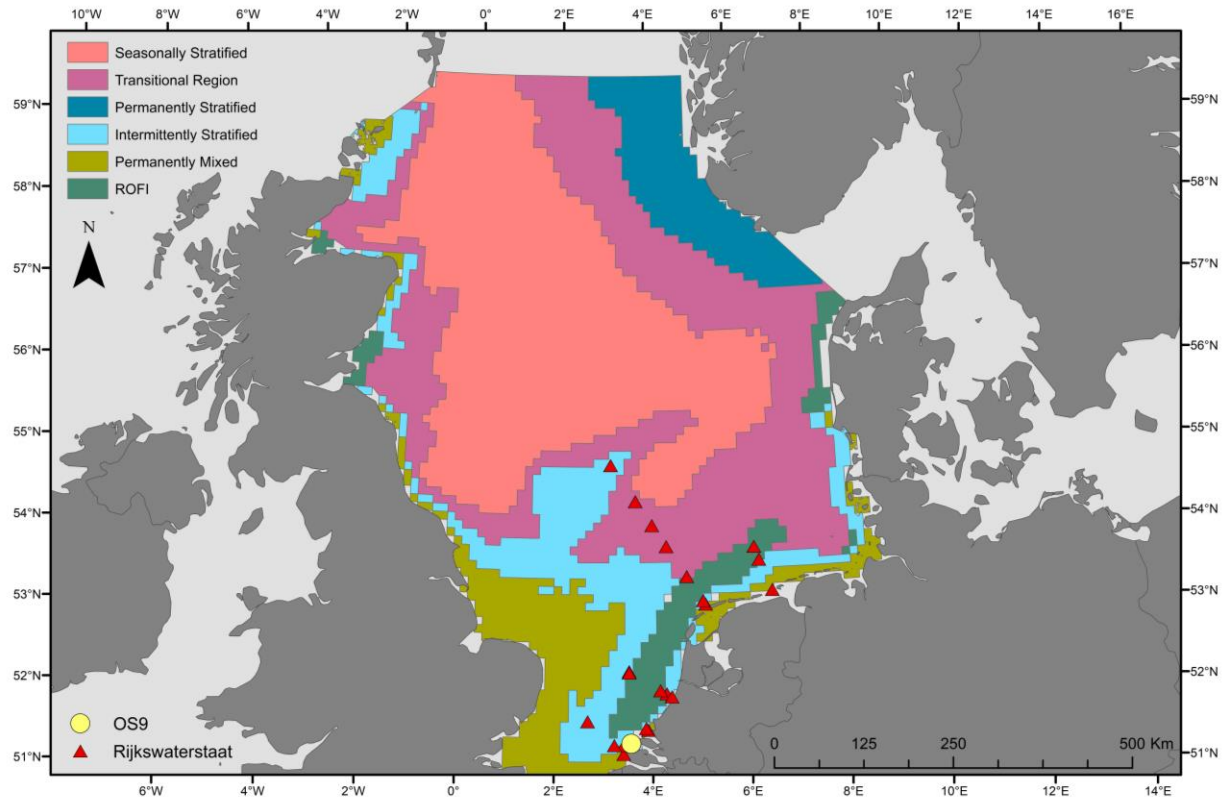
Figure 4: Map of the hydrodynamic regions classified by the rho density in the North Sea (shapefiles from van Leeuwen et al., 2015). The coordinates of the OS9 and Rijkswaterstaat data points are also illustrated in this figure

2.3 Satellite imagery and processing
2.3.1 *Water quality parameter retrieval from MERIS*

The satellite images used were taken by MERIS, a Medium-spectral Resolution, Imaging Spectrometer, an instrument onboard Envisat. Envisat is a sun-synchronous satellite with data available for download spanning the period 17/05/2002 - 08/04/2012 (ESA, 2012). Unique acquisition dates between 2002-2012 matching the water quality

parameter datasets from the Rijkswaterstaat were compiled these images were downloaded via the CoastColour website (http://www.coastcolour.org/ccprocessing/calvalus.jsp). MERIS is an imaging spectrometer with spatial resolution of 290m x 260m and has relatively high spectral resolution between the wavelength spectrum of 390-1040nm with approximately 15 spectral bands. CoastColour is an ESA (European Space Agency) project set up to process MERIS images specifically for addressing the issue of classifying Case 1 (open ocean) and Case 2 (coastal zones) waters. The CoastColour project developed region-dependent and parameter-specific algorithms to better translate wavelength spectrum and the corresponding values for each water quality parameter. CoastColour provides products of three processing levels: Level 1 processing involves atmospherically correcting raw satellite imagery to account for Top of Atmosphere (TOA) reflectance and scatter. Level 2 images consists of environmental parameter datasets, calculated using the neural network algorithms developed for the CoastColour project, which involves an inverse modelling technique that is first trained with reflectance data to produce the inherent optical properties (IOP) of water, instead of training the neural network with IOP values and generating potential reflectance data (Brockmann Consult, 2014). The neural network is also optimized for different regions and water type, and is trained using the MERis Matchup In-situ Database (MERMAID, http://mermaid.acri.fr/dataproto/dataproto.php). Finally, Level 3 processing involves a combination of more than one image in order to generate an average composite image of a specified period, or a mosaiced dataset to provide a complete picture. Although Level 2 and Level 3 images were downloaded for this project, only Level 2 images were used in this study as Level 3 images of monthly periods were found to contain missing pixels from the individual parameters despite pixel value availability in Level 2 images from within the same period. Therefore, self-composited level 3 images were generated for every month in each year using the Cell Statistics function in ArcGIS 10.5.

The water quality parameters used in this project from Level 2 images are the neural network derived chlorophyll-a concentrations (chl-a), light attenuation coefficient at 550nm (K_d) and Suspended Matter Concentrations (SPM). Although the BPI model does not include SPM, the SPM products from MERIS were validated in any case. Due to the limited data available, the possibility of modelling light attenuation K_d from SPM was considered based on Devlin et al. (2008).

2.3.2 *Surface irradiance E_o*

To calculate surface irradiance data, downward shortwave radiation flux was needed. This was taken from NCEP Reanalysis 2, a global radiation budget model from NOAA (https://www.esrl.noaa.gov/psd/data/gridded/data.ncep.reanalysis2.html). As the units are in W/m^2, conversion to molphotons/m^2/day (or E/m^2/day) was performed, following

Capuzzo et al. (2017). First, to account for reflection and scatter from the surface of water bodies, a value of 0.95 was applied onto the downward shortwave fluxes (5% reflection). To further account for the total amount of Photosynthetically Active Radiation (PAR) available, the flux values were multiplied by 0.45 (45% of sea surface irradiance as PAR from Kirk, 1994). Next, to convert W/m^2 into photon irradiance, a conversion factor of 4.15*10^{-6} was applied, and this is explained in the equations below, which was taken from Morel & Smith (1974).

$$1 J = 1 Wm^{-2} = 2.5 * 10^{18} \ quanta$$

$$1 \ quanta = 1.66 * 10^{-24} Em^{-2} day^{-1}$$

$$1 Wm^{-2} = (2.5 * 10^{18}) \times (1.66 * 10^{-24}) = 4.15 * 10^{-6} Em^{-2} day^{-1}$$

Lastly, to account for the total daily photon irradiance, the values were multiplied from 3600 (for minutes and seconds), and further multiplied by the daylength (hours). As daylength differs every day and for different latitudes, the approximate coordinates for the North Sea from the North-South intersecting with the East-West lines are taken, which was found to be 3°E 36', 55°N 30'. By doing so, the final primary production values generated therefore assumes that daylength is uniform throughout the North Sea. Of course, differences of daylength are approximately ±25 minutes from the midway point to the Northern or Southernmost point of the North Sea. Therefore, pixel values derived further away from the latitudinal midpoint will have a higher error margin caused by the difference in daylength as opposed to pixel values which are closer to the latitudinal midpoint. This amounts to the final primary production (PP) value having a potential maximum error of margin of up to ±(0.0015*PP). Additionally, the error of margin changes throughout the year due to the effect of seasonality on daylength period.

2.3.3 *Standardized anomaly of primary production*

After deriving monthly averages of primary production in the North Sea between 2002-2012, standardized anomalies were generated of each region throughout the period to test for changes in primary production through time. The calculation of standardized anomalies is shown below, where x_{yr} is the daily mean primary production averaged for a particular year, μ is the average of daily mean primary production throughout the years and σ_{yr} is the standard deviation of the daily mean primary production for a particular year.

Equation 5

$$Standardized \ anomaly = \frac{x_{yr} - \mu}{\sigma_{yr}}$$

3 Results

3.1 Calibration of BPI model using in-situ measured data from station OS9

The BPI model was calibrated using in-situ data from station OS9. 8 sample points from OS9 were available for use as input for the model calibration. These samples were taken between the years 2007-2008, and the primary production data is shown in the figure below.
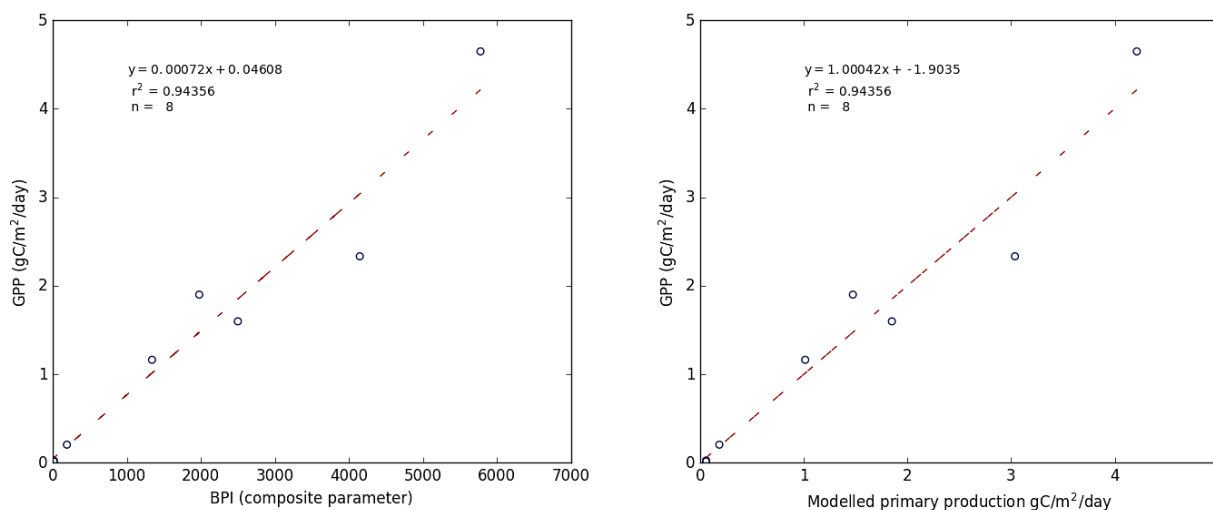
Figure 5: (Left) BPI model applied onto the OS9 dataset. (Right) Modelled primary production values compared against ^{14}C measured GPP values

Figure 5 (left) shows the results of the BPI model applied onto the OS9 dataset. The resulting correlation coefficient between the BPI composite values and measured primary production values yields a significant value of r^2 = 0.944 (p-value = 5.74*10^{-5}) (*see appendix for linear regression analysis graphs*). Using the equation derived from Figure 5 (left), i.e. *y = 0.000721x + 0.0461*, this was used to predict primary production. Predicted values were calculated and regressed against measured GPP values, as illustrated in Figure 5 (right). The slope (*1.0004*) of the regression between predicted and measured production values shows an almost exact relationship. To investigate if the model could be further improved, calibration of the *a* and *b* terms were performed. However, no further improvements could be made to constrain the model further. Variations of the model were made by adding another parameter to the model: P_{max}. By testing the BPI*P_{max} model, Figure 6 shows the results of the regression between the BPI*P_{max} composite parameter and measured GPP values. The correlation coefficient yielded a high r^2 value of 0.96 (*p-value*: 2.25*10^{-5}),

demonstrating a significant relationship with measured primary production values. Considering the strong relationship Pb_{max} contributes to with GPP, this parameter can also be obtained by modelling it using temperature-dependent models i.e. Behrenfeld & Falkowski (1997b), Morris & Kromkamp (2003) and Cox et al. (2013). Unfortunately, this was not possible in the project as there were insufficient temperature measurements from station OS9, with only 6 out of 8 samples having temperature data. Since the OS9 dataset was already limited, a further decrease in available temperature measurements restricted the ability to conduct a reasonable and validated estimation of the Pb_{max} parameter and subsequent calibration. Furthermore, results of ANOVA performed on the dataset shows that the residuals increase if the BPI*Pb_{max} is used, as compared to the BPI model alone (see *appendix 8.3 pg 56*). Additionally, the r^2 values from using the BPI model versus the BPI*Pb_{max} model do not differ by much, hence, the Pb_{max} parameter was not included as part of the model used for the results of the study.
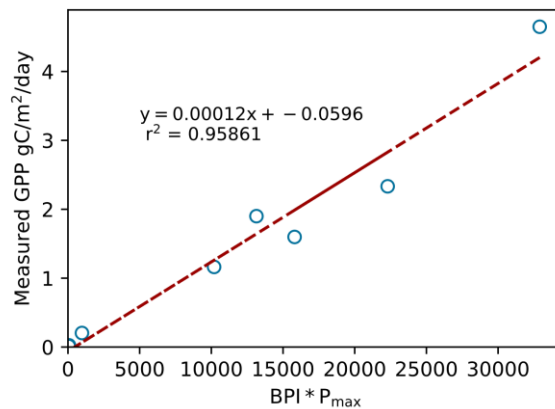
Figure 6: BPIPb_{max} composite parameter regressed against in-situ measured GPP values*

3.2 Validation of water quality parameters

3.2.1 *Validation of satellite-retrieved water quality parameters for station OS9*
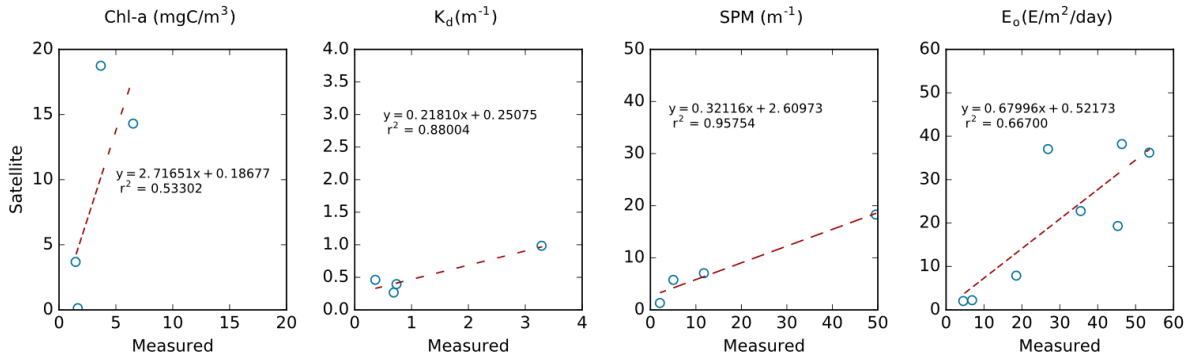
Figure 7: Comparison of measured versus satellite derived values for the various water quality parameters. Surface irradiance Eo (far right) values from the NCEP Reanalysis 2 model are compared with measured values taken from the NIOZ-Yerseke radiance sensor

To assess the reliability of using OS9 as a station for calibrating the BPI model, water quality parameters (chl-a, K_d, SPM) were retrieved from the MERIS images for the dates coinciding with the sample dates of OS9, while daily surface irradiance E_o was taken from NCEP Reanalysis 2, a global radiation budget model from NOAA. Taking into mind that only 4 images were found to coincide with the OS9 sample dates for the water quality parameters, therefore, only 4 data scatter points are illustrated for each water quality parameter in Figure 7. For E_o, as the model had daily average values available, all 8 values were found for all sample dates in OS9 and are illustrated in Figure 7 (right). Considering the very small sample size for the three water quality parameters, the r^2 values may not be reflective of the performance of the MERIS parameter algorithm.

Satellite-derived chl-a has a wider range of values (18.6) compared to measured values (5.1). Furthermore, 3 satellite-derived data points were over-estimated by almost three times as much as measured in-situ chl-a values, apart from one value which was under-estimated by 12.6 times the measured value. Satellite-derived K_d values, on the other hand, have a much smaller range of values than measured K_d values. Values fall between 0.27-0.98, while measured values fall between 0.36-3.29. All values of K_d were under-estimated by approximately 5 times the value in the MERIS images. Consequently, the high regression found for K_d is driven by a single point, as three of the data points are clustered near each other. Similarly, satellite-derived SPM values also had a smaller range than measured values, with satellite values falling between 1.3-18.3 while measured values fell between 2.1-49.6. Most values were underestimated as well by an order of approximately 3 times less than measured values. Regression of measured and modelled E_o values returned an r^2 value of 0.67 (*p*-value = 0.0134), with modelled values falling between a range of 2.05-38.2 $E/m^2/day$,

while measured values were between a range of 4.5-53.6 $E/m^2/day$. Furthermore, values are generally underestimated, as most values fall below the regression line in Figure 7 (right), apart from two values.
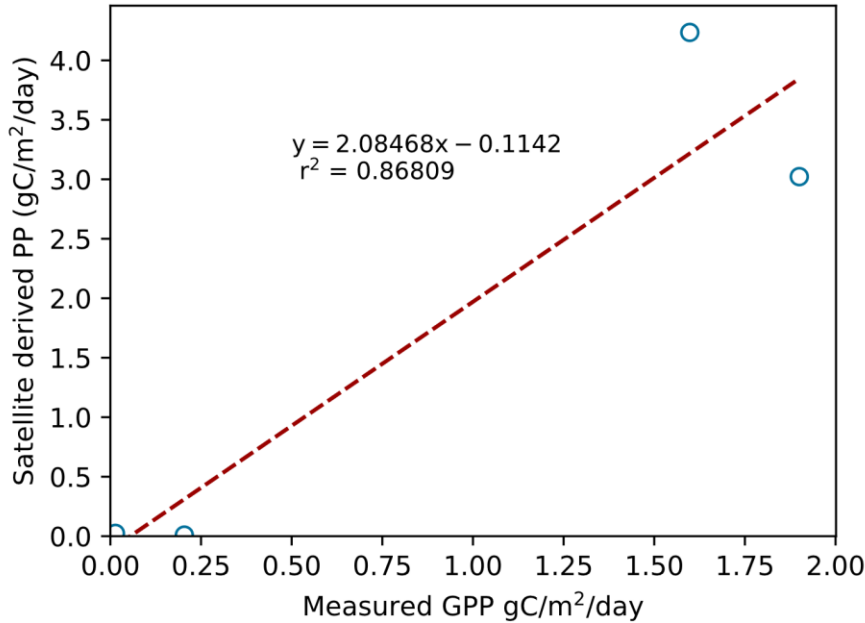
Figure 8: Comparison of primary production values from measured and satellite-derived data for OS9. No correction factor applied onto dataset yet.

The BPI model was applied onto OS9 images and primary production was calculated. No correction factor for the satellite-retrieved water quality parameters was used yet as the reliability of the retrieval could only be assessed by validating the satellite values with the Rijkswaterstaat station data later on. The results are illustrated in Figure 8**Error! Reference source not found.**, where it can be observed that satellite-derived estimates of primary production appear to overestimate measured values by a factor of 2. Although the r^2 value is high (0.87, *p*-value = 0.068), there are only 4 data points available for validation in OS9. The *p*-value derived shows that this relationship is less likely to be significant, but without more data availability, validation is difficult to perform.

3.2.2 *Validation of satellite-retrieved water quality parameters for Rijkswaterstaat stations*

Results of the comparison between satellite-retrieved and in-situ measured water quality parameters at the Rijkswaterstaat stations are illustrated in Figure 9. The correlation coefficient and equations are further summarised in Table 2. In summary, water quality parameter retrieval from satellites performed reasonably well, with r^2 values of more than approximately 0.5. The *p*-values of all water quality parameter regressions indicate that the results are not due to random chance, and therefore significant regressions. Additionally, the F-statistic values are well over the *F* critical values of 99.99% confidence levels for all parameters. The parameter with the lowest regression coefficient value was SPM ($r^2 = 0.5$), yet, the r^2 value does not differ much from chlorophyll-a ($r^2 = 0.51$) either. Light attenuation coefficient K_d performed the best, with high r^2 values of 0.75. In addition, both light attenuation coefficient and SPM values were, in general, underestimated by twice the amount. Chlorophyll-a values have an almost exact relationship between satellite and measured datasets (slope = *1.1*).

Table 2: Table of water quality parameters with the respective equations (y = satellite, x = in-situ values) and regression coefficients of the regression

Parameter	Equation	Regression coefficient (r^2)	P-value
Chlorophyll-a	$y = 1.097x + 1.01150$	0.514	$< 2.2 * 10^{-16}$
Light attenuation coefficient K_d	$y = 0.48x + 0.01139$	0.75	$1.929 * 10^{-15}$
SPM	$y = 0.517x - 0.59$	0.497	$< 2.2 * 10^{-16}$

In general, for all measured and satellite-derived in-situ water quality parameters (blue circles and red triangles respectively in Figure 9), higher values were found closer to the shore than further offshore. The range of values also decrease by a magnitude smaller from 2km to 200km offshore. In addition to the decrease in values from the coast, it can also be observed that only chl-a satellite-derived values fell within the similar range found in measured values, unlike SPM and K_d, for which satellite-derived values were at a visibly lower range than measured values. In view of the under-estimation found for the light attenuation coefficient parameter, a correction factor of 0.48 was applied onto satellite images for primary production modelling later. To further test if log-transforming the data would improve correlations, Figure 9 also features the regression between $\log_{10}$-transformed measured and satellite-derived values of each water quality parameter (middle column). For chl-a, the regression significantly worsens by 0.2, although the relationship is still mostly a 1:1 regression. For K_d, the r^2 value remains approximately the same, and for SPM, the r^2 value improves by 0.12.
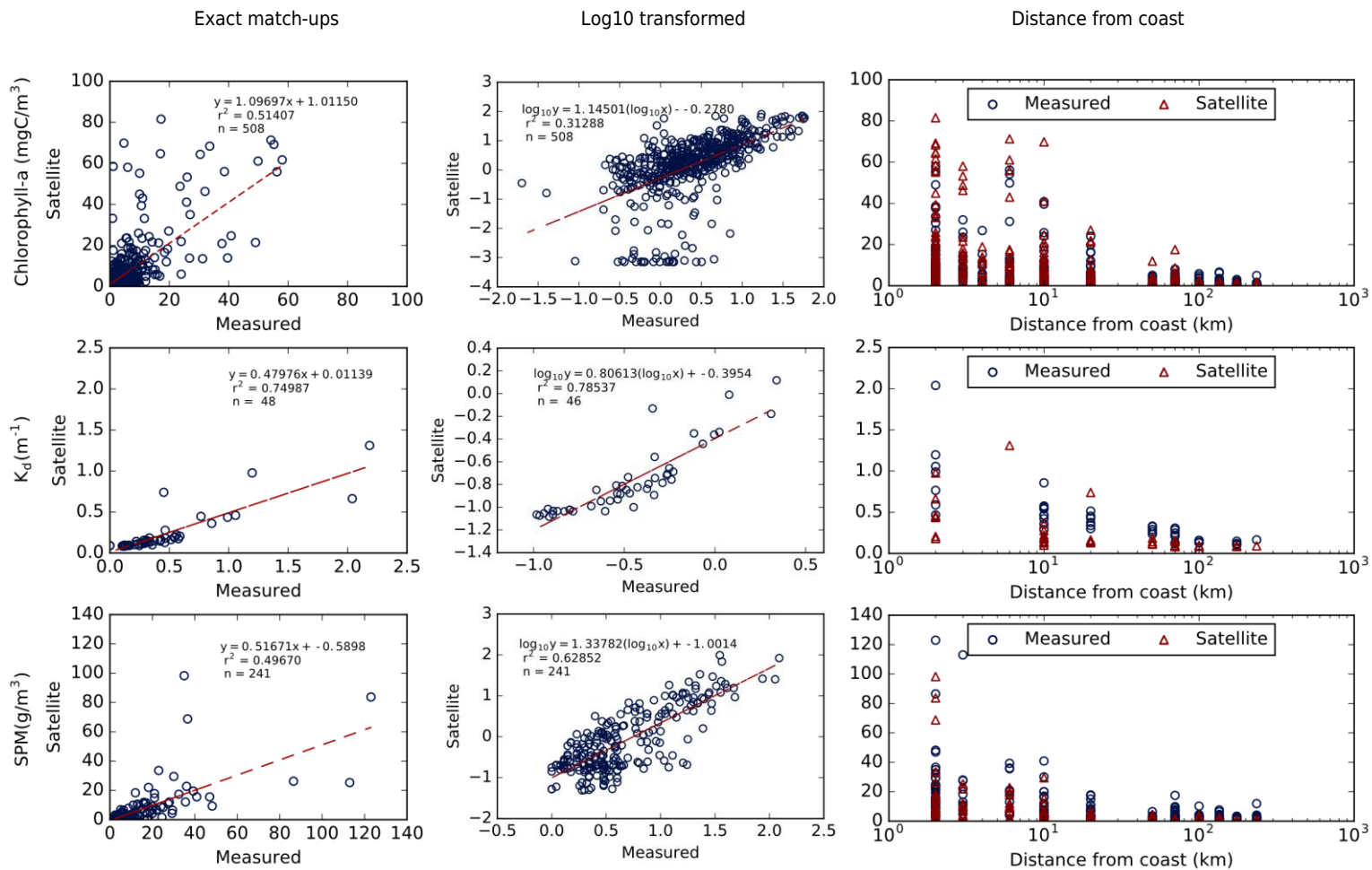
Figure 9: Comparison of water quality parameters derived from measured values (obtained from Rijkswaterstaat*) and MERIS. The left plots show a direct comparison of measured versus satellite-derived datasets, the middle plots show a direct comparison of $\log_{10}$- transformed datasets between measured and satellite-derived values, while the right plots show comparison of values based on the distance from coast [Note: distance from coast(km) is plotted on a logarithmic scale]. Top: chlorophyll-a (mgC/m³); Middle: light attenuation coefficient K_d (m⁻¹); Bottom: Suspended Matter Concentration SPM (g/m³)*

Additionally, the log-transformed chlorophyll-a comparison between measured and satellite-derived values show a number of satellite-derived values that lie along the same values i.e. approximately -3. Although these seem to be outliers, the neural network calculated low values for chlorophyll-a, which explains why the values are approximately -3 once it is log-transformed. However, none of these values were found beyond the Cook's Distance Line during linear regression analysis, suggesting that despite appearing to be outliers, there is statistically not enough reason to remove them from the dataset for analysis.

To further investigate the significance of the measured versus satellite-derived values of each water quality parameter, linear regression analysis was performed on the datasets of each individual parameter, and the results are illustrated in Figure 10. For datasets to be considered having a normal distribution, most sample points should fall in a horizontal band across the value 0 in the 'Residuals vs Fitted' plots. As observed, most data points tend to cluster towards the left side of the plot, or the lower values. The red line represents a general trend of fitted values against residuals, and while the trendline for chl-a is a straight, horizontal line near the value 0, this is not observed to be the same for K_d and SPM, as a kink in the trendline is found. In addition, the kink in the trendline is steep at the lowest values in the dataset, suggesting a general skew. Quantile-Quantile (Q-Q) plots visually illustrate the distribution of datasets. A dataset with a normal distribution should show data points falling along a straight line. This is however, only observed for K_d, while chl-a and SPM both show an 'S'-shaped curve. Curved tails in Q-Q plots are also known as "heavy-tails", which may indicate that data is not normally distributed, and might exhibit extreme values at the end-member range (i.e. minimum and maximum). Scale-Location plots help test the assumption that data exhibits homoscedasticity, with data points falling along a roughly horizontal straight line in the plot assuming equal distribution of similar variances. As observed, none of the scale-location plots display a horizontal straight line. The scale-location plot in chl-a shows a diagonally straight line, which may indicate lower residuals found in lower fitted values, while residuals increase proportionally with fitted values. The scale-location plot for K_d shows a peculiar kink in the trendline, indicating an unexplained variation in variance at lower fitted values. The scale-location plot for SPM displays a diagonal line, which exhibits a slight kink at lower fitted values. The gradient of the kink may suggest that the margin of error increases strongly with small increases in SPM values. Residuals vs Leverage plots contain Cook's distance lines, and data points lying beyond these lines have a likelihood of being classified as an outlier which has the potential to significantly influence regression results. By comparing all the Residuals vs Leverage plots from each parameter, this may help indicate consistent outliers occurring across datasets, removing them from analysis if needed. Based on the results of these plots, while outliers exist in the datasets of these parameters, they do not consistently occur throughout, as parameters with similar image dates do not exhibit the same outliers as the rest.

Lastly, to investigate if the distribution of datasets could be further improved by transforming them, linear regression analysis was also performed on the $\log_{10}$-transformed datasets (refer to Supplementary 9 for linear regression analysis plots of the $\log_{10}$-transformed datasets). The results of transforming the datasets does not significantly improve the distribution of data. The residuals vs fitted line does not fall along a horizontally straight line for all water quality parameters, instead, they follow a quadratic curve that suggests a non-normal distribution in the dataset. In the Q-Q plots, only chl-a displays a normal distribution, however, K_d displays some heavy tails that were also found in the linear regression analysis of the non-transformed datasets. SPM additionally displays some skew at lower values in the Q-Q plots, suggesting some level of heteroscedasticity. Scale location plots are also not quite exactly a horizontal band, with large scatters and the trendline appears to be wavy. Yet, there are no obvious outliers present in the data as none of the points are located beyond the Cook's Distance lines. In summary, transforming the dataset does not necessarily improve the distribution of data, therefore, calibrating the model based on the transformed dataset was not necessary.
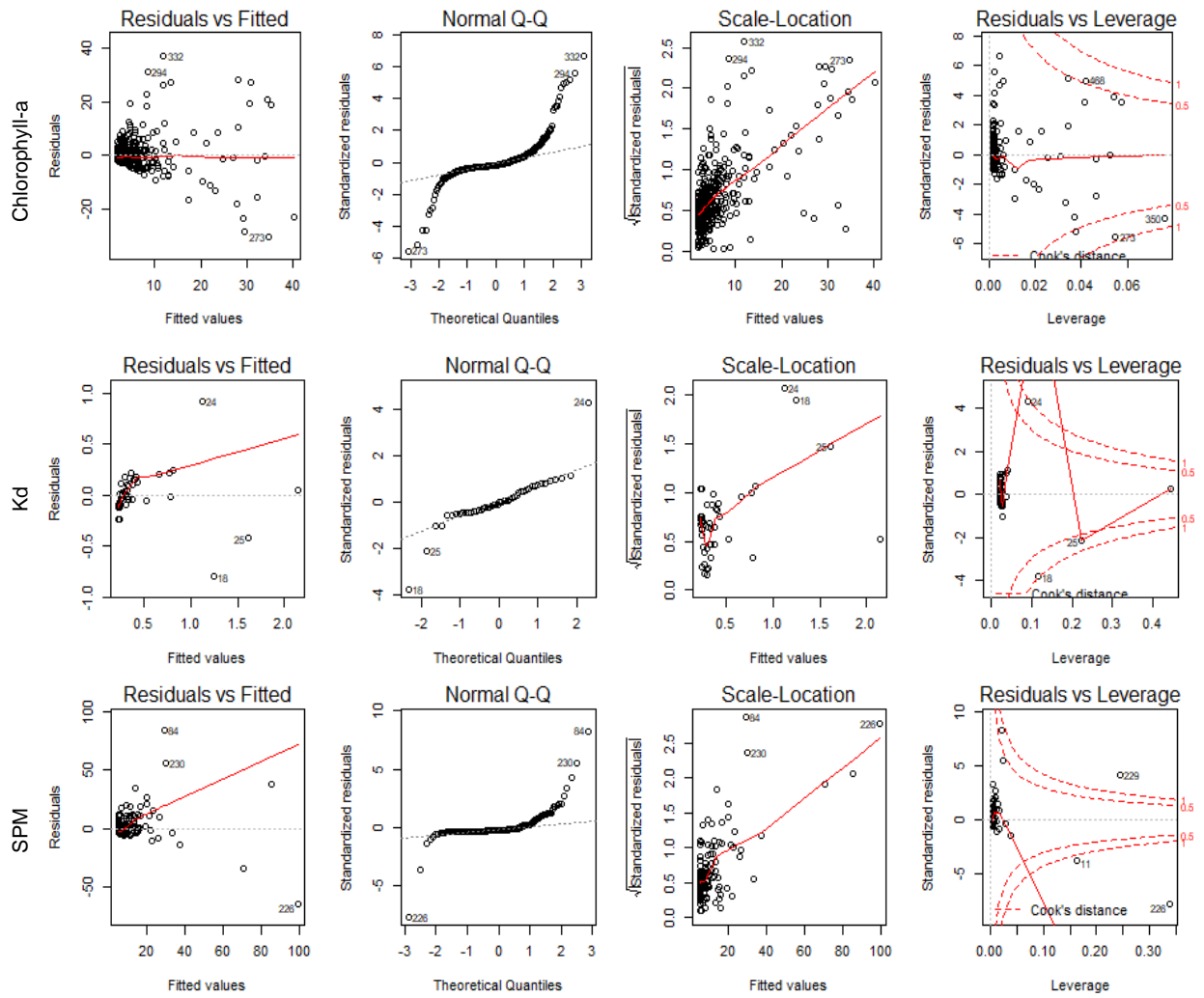
Figure 10: Linear regression analyses of the water quality parameters (Measured versus satellite-derived values). Top: chlorophyll-a; Middle: K_d; Bottom: SPM
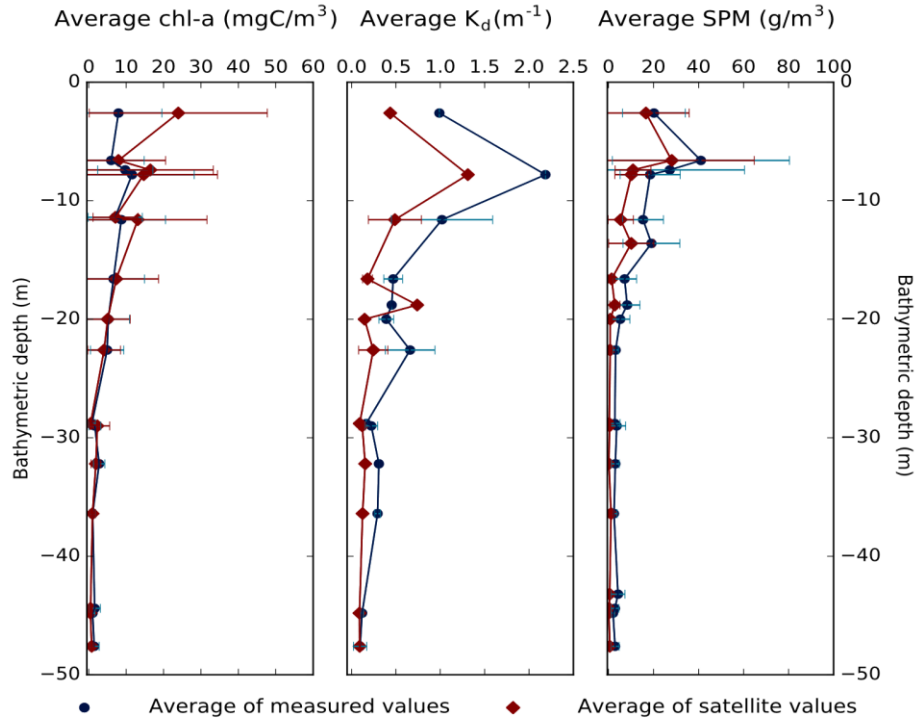
Figure 11: Comparison of averaged measured vs satellite-derived values of the water quality parameters versus bathymetric depth. Averaged values were derived by averaging all match-ups that have similar depths. Error bars indicate standard deviations of points.

Measured and satellite-derived water quality parameters were plotted against bathymetric depth (Figure 11). The underestimations observed for the satellite-derived K_d and SPM values in Figure 9 are also apparent in Figure 11. In general, all parameters displayed a decreasing trend towards areas with greater bathymetric depths. The standard deviations are also observed to decrease as bathymetric depth increased, with the largest standard deviations observed to occur at shallower depths. For all parameters, values were observed to increase slightly at around 6-8m depth before continuing on a decreasing trend. This trend occurs in both measured and satellite-derived datasets. For chl-a, both measured and observed datasets display the same trends in data, although satellite-derived chl-a values at shallower depths appear to slightly overestimate measured values before returning to roughly similar values at greater depths (>30m onwards). Additionally, chl-a concentrations are first observed to decrease between 2.6-6.6m depth, before increasing slightly and then decreasing again. For K_d, both satellite-derived and measured values show an initial increase of 1.19 m^{-1} and 0.87 m^{-1} respectively, before decreasing in general. It must be noted that this initial increase in Kd values may not be significant and representative of how light attenuation varies with bathymetric depth as the data point has no standard deviation, indicating that the average value derived for that point was only an average of one match-up point. Lastly, both measured and satellite-derived SPM values first shown an increase in values before decreasing. The relatively steep decrease in values between 6.6-7.4m depth appears to coincide with the small increase in chl-a concentrations observed.

3.3 Primary production for the North Sea between 2002-2012

3.3.1 *Monthly composites of primary production in the different hydrodynamic regions*

Figure 12 illustrates a time-series curve of monthly primary production data from each hydrodynamic region in the period 2002-2012. As can be observed, primary production in all regions exhibit an annual variation in production trends. The lowest values typically occur between October-February, while the highest values occur between the April-July months. The hydrodynamic region that has the lowest mean peak primary production values over the period is the seasonally stratified region, followed by the transitional region. The highest mean primary production values occur in both the region of freshwater influence (ROFI) and the permanently mixed region, at a value of 1.3 gC/m^2/day. In the case of some regions, a double peak in primary production values during the spring-summer months (April to July) was observed in the satellite data. For example, the seasonally stratified region shows double peaks in primary production in the years 2002-2004 and 2011. The first primary production peak starts to occur around April, where it reaches maximum values typically around May before decreasing. The second peak occurs during the onset of the autumn months, between September and October. In the case of the intermittently stratified region, it does not appear to exhibit the double peak trend in primary production values throughout all years. Lastly, the timing of the peaks does not occur at the same time for all regions. Most regions tend to have their peaks coincide around the same months, sometimes a month earlier or later instead. For most regions, 2006 was the year in which the lowest peak primary production values were reached during the entire period of analysis. For 2010, the ROFI experienced its lowest peak mean primary production value throughout the entire period, while the seasonally stratified region experienced its highest peak production value. In addition, the transitional region also experienced its lowest peak values in 2010.

Annual primary production per square metre for each region was calculated by multiplying the daily mean for each month by the number of days in the month and summing all the months for the year together. This is illustrated in Figure 13. Annual primary production values are lowest for the seasonally stratified region, followed by the transitional region. The highest annual primary production values belong to the ROFI and followed closely by the permanently mixed region. The dip in primary production values for the year 2006 that was observed in Figure 12 also occurs in the annual primary production values, with the exception of the seasonally stratified region where the fall in primary production value appears to occur a year earlier than the rest of the regions, and the transitional region. Between the years 2003-2005, most regions appeared to face decreasing annual primary production values except for the permanently stratified region. Annual primary production values for that region remain around similar values before declining in 2006.
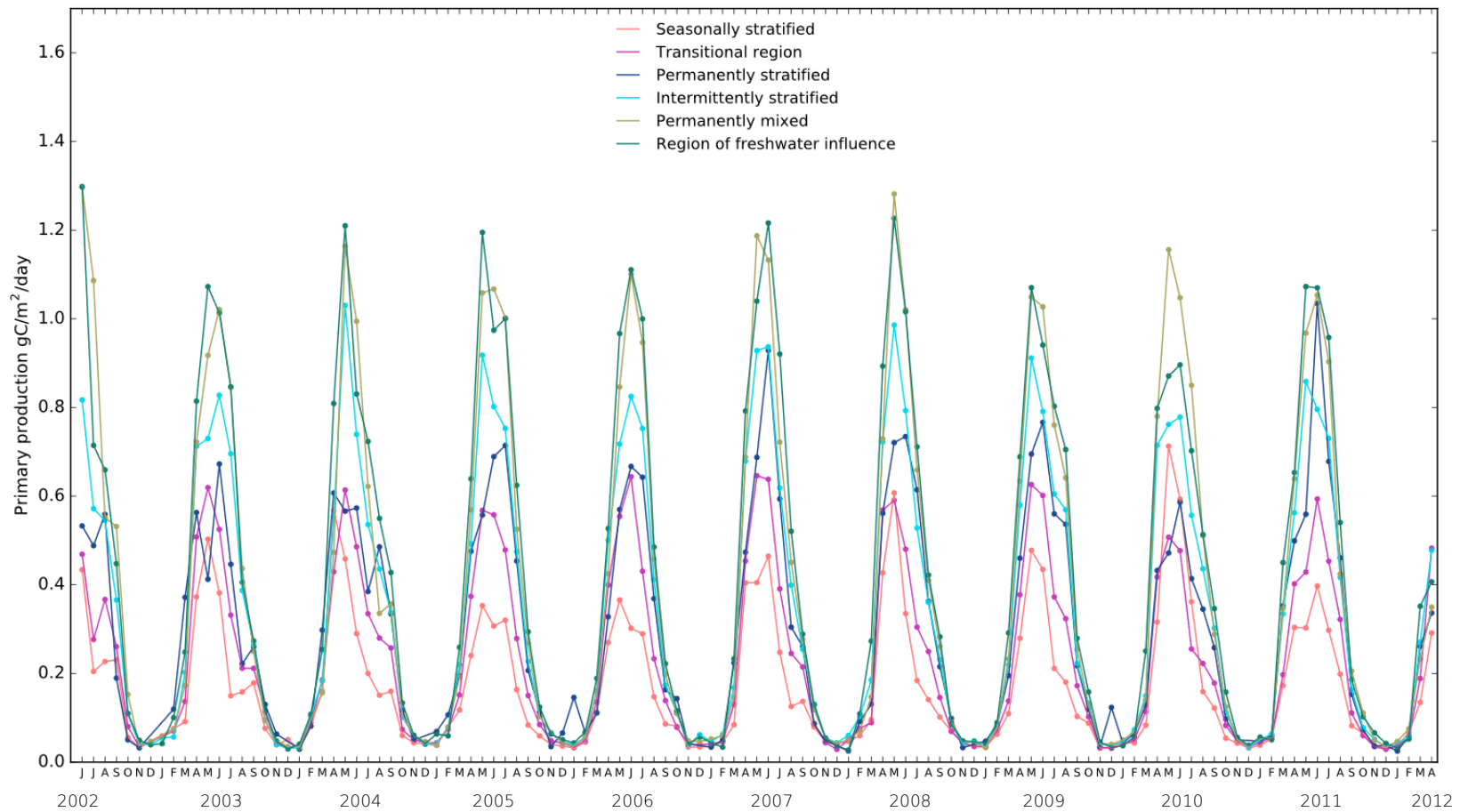
Figure 12: Monthly primary production modelled based on satellite data of the 5 hydrodynamic regions in the North Sea between 2002 and 2012
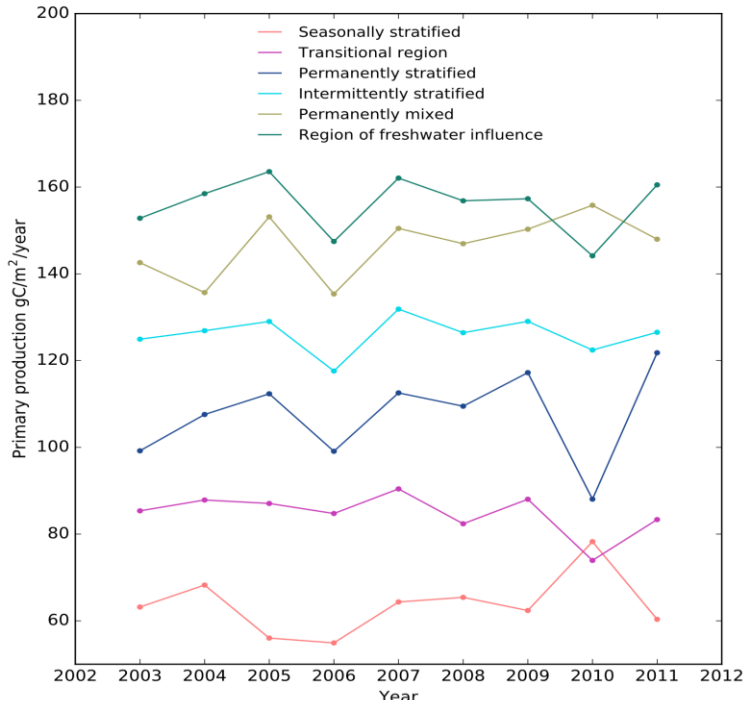
Figure 13: Annual primary production modelled based on satellite data for each hydrodynamic region per square metre between 2003-2011. 2002 and 2012 was discounted from the calculations due to lack of sufficient monthly data
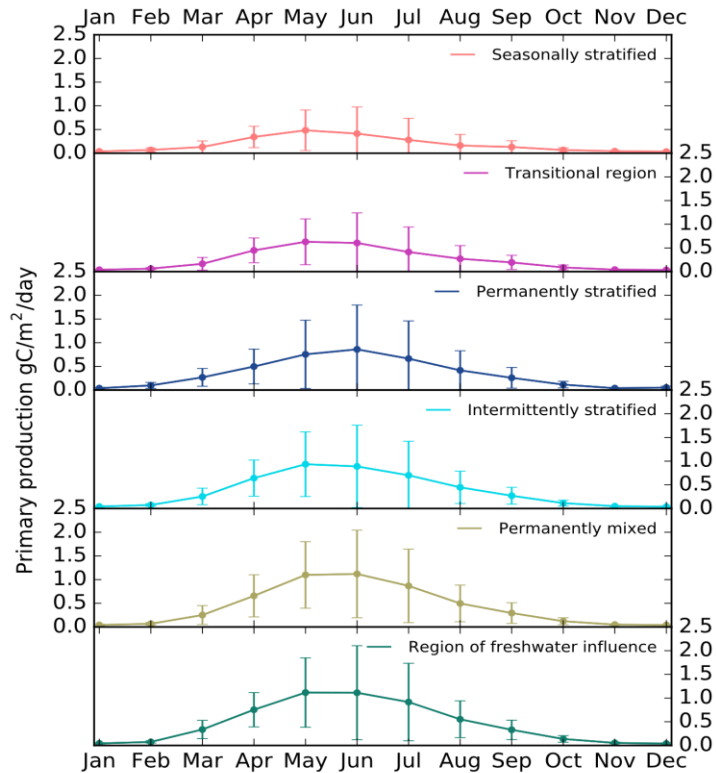
Figure 14: Overall daily mean primary production values for each month averaged over the entire period (2002-2012) modelled from satellite data. Error bars indicate standard deviations.

Between the years 2003-2011, the intermittently stratified, permanently stratified and ROFI regions share similar trends in primary production values, even with the large decrease in annual primary production values in 2006 and 2010, though the decrease in 2010 for the intermittently stratified region was much less so. From 2007 onwards, the transitional region also shared similar trends in annual primary production values with the ROFI, intermittently stratified and permanently stratified region. On the other hand, the permanently mixed and seasonally stratified region experienced an increase in annual primary production values (per square metre) in 2010, unlike the other regions. The permanently stratified region faced the largest decrease in annual primary production values in 2010, falling by almost 40 gC/m^2/year before increasing again in 2011 and returning to a similar value as in 2009.

The overall monthly averaged daily primary production values for each region are illustrated in Figure 14. The intermittently stratified and permanently stratified regions do not have the highest daily mean production values for each month, yet, the standard deviations are highest. This suggests a variable

spread in data values due to spatial heterogeneity. The overall monthly average for the entire period for all regions between 2002-2012 obscures the double peak signals observed in Figure 12. Most regions, instead, appear to show a maximum peak occurring in the spring or summer months. For most regions, the bloom occurs in May, and this includes the seasonally stratified zone, ROFI and intermittently stratified region. For the permanently stratified and permanently mixed area, the similar peak values are found for both these regions, although the exact timing of the peak is less clear as both May and June have roughly similar values. The transitional region shows no clear peak differences for the months of May and June. To further investigate overall differences in primary production amongst the regions, a box and whisker plot was made of the overall monthly primary production values averaged over the entire period. The lowest median, maxima and smallest interquartile range is found in the seasonally stratified region while the highest median, maxima and largest interquartile range is found in the ROFI. Although the interquartile range of the permanently stratified zone is significantly smaller than the interquartile ranges of the permanently mixed and intermittently stratified zone, the median values are approximately similar for these three regions. The results in the box and whisker plot appear to correlate well with the results from Figure 12 and Figure 13.

A cumulative view of the annual primary production integrated over the year and area is illustrated in Figure 16, where the proportion of primary production contributed by each region to the annual North Sea production budget is shown. Despite having the highest mean production values per year for most months, the ROFI contributes as one of the least to the annual production budget. The permanently stratified region showed large changes in primary production through the years per square metre, yet, it shows one of the smallest changes through time when integrated over the year and area. Furthermore, although the seasonally stratified region is consistently observed to have the lowest mean production values amongst the other regions, it contributes as one of the highest to the annual production budget, along with the transitional region. The permanently stratified region and the ROFI contributes the least amongst all regions. Although some variation in mean values across the period is observed (refer to Figure 13), by calculating the total contribution of production across the area of the different hydrodynamic regions, some of the main trends in mean production values observed are not necessarily reflected in the area-integrated values. For example, the ROFI experienced dynamic changes in annual production values, with a decrease of almost 20 gC/m^2/year in 2006 and another decrease in production value in 2010. These troughs in production values are not observed in the area-integrated results, instead, it appears that the area-integrated values remain roughly constant through the decade. The decrease in primary production values for 2006 observed in some of the results mentioned earlier can also be observed to have a significant impact on the annual production budget for some of these regions, particularly affecting the seasonally stratified region the most. In Figure 13, the seasonally stratified and permanently mixed had an observable increase in annual mean production values. Yet, the area-integrated values in Figure 16 show a sharp increase for the seasonally stratified zone, and much less so for the permanently mixed zone. Therefore, results show that despite dramatic changes in mean annual

production values per m^2, the total area of a region is also important in determining the total contribution to the annual primary production budget of the North Sea. In addition, despite the decrease in annual primary production per square metre in 2010 for 4 of the hydrodynamic regions, it can be clearly seen that the seasonally stratified region makes up for that decrease, resulting in no change occurring in 2010 for the primary production budget of the entire North Sea. The only prominent change to the North Sea primary production budget is in 2006, however, that change is recovered in the next year already. To test whether there was any significant trend in North Sea primary production for the time period, linear regression analysis was performed on the annual total budget of the North Sea between 2003-2011. Results showed an increasing slope (*y = 0.1x – 155.95*) with an r^2 value of 0.0425 (*p*-value = 0.595).
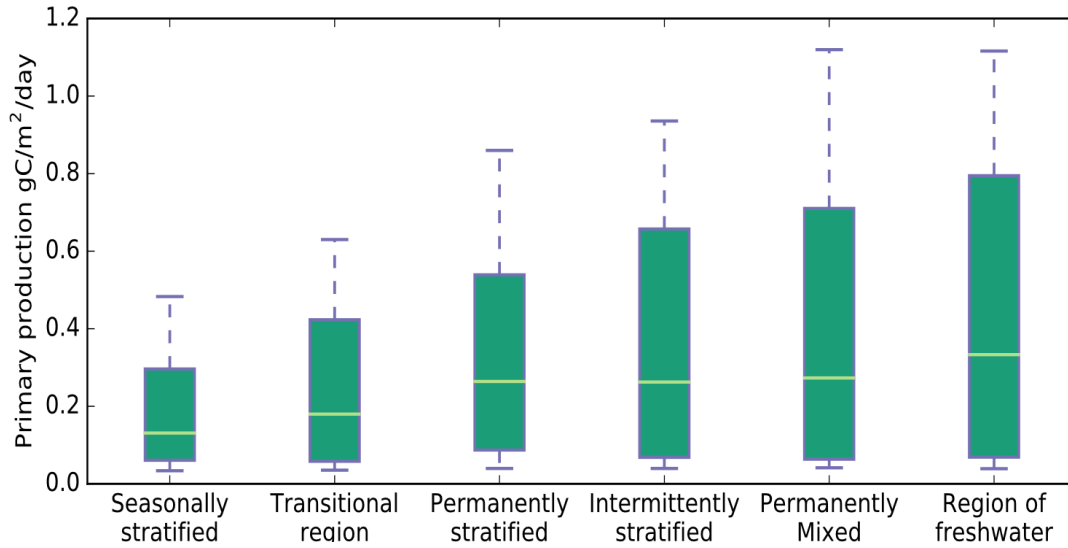
Figure 15: Box plot of the distribution of the overall averaged monthly primary production values across different hydrodynamic regions. The box plot features the median, maximum, minimum and interquartile range of the overall monthly average primary production.
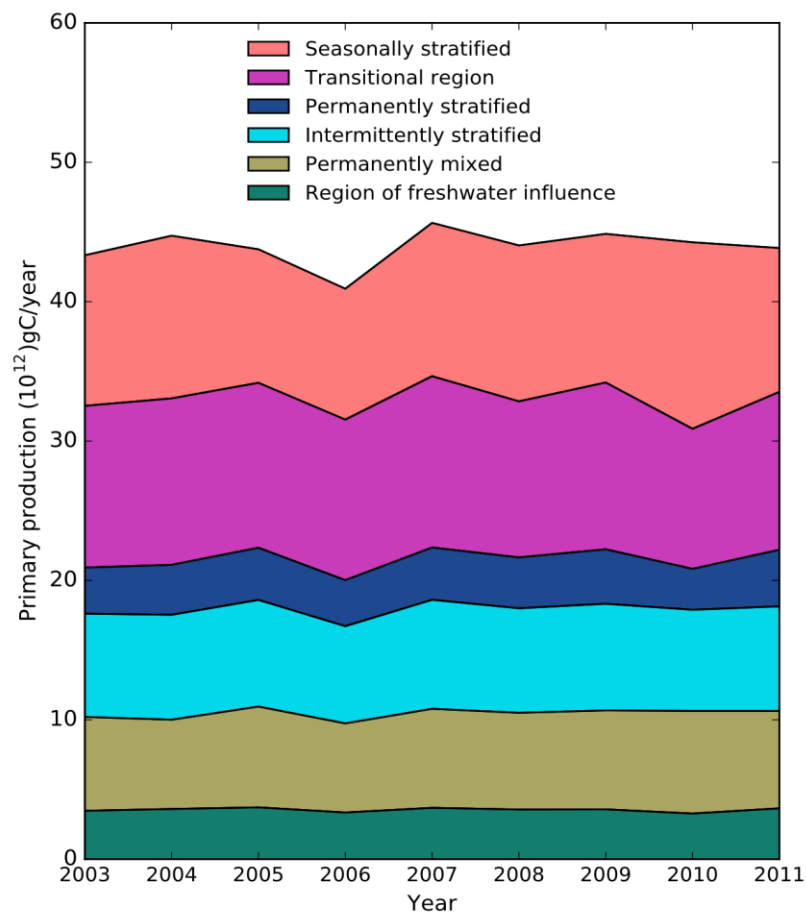
*Figure 16: Annual production per year for the entire hydrodynamic region plotted cumulatively atop each region (Area * mean annual PP). Therefore, this figure also features the total primary production budget of the entire North Sea region (total area of 469537km2 based on van Leeuwen's shapefiles).*

To assess how primary production in the North Sea changes through time for each region, a standardized anomaly of mean primary production values per year was made (Figure 17). A value of 0 for the standardized anomaly serves as the overall mean production line, and therefore, the positive or negative anomalies represent deviations from the standard mean value with reference to each year. This helps to deduce if production values are deviating further than normal or remaining approximately similar through the years. Results show that the region displaying the highest deviations, including both positive and negative anomalies, is the seasonally stratified region, while the region with the least observed deviations is the ROFI. In all regions during 2006, larger than normal negative anomalies occurred. This supports previous observations that 2006 experienced a dip in primary production. Although the annual time-series results showed that this dip in primary production may have already occurred earlier for the seasonally stratified region, the annual primary production values for 2006 were still lower than average as the region still experienced a negative anomaly for that year. Overall, between the period of 2003-2011, years that faced anomalously large changes in primary production is 2006 and 2010. Although all regions share similar anomaly trends for 2003, 2004 and 2006, the anomaly behaviour is not necessarily consistent with each year when comparing regions with each other.
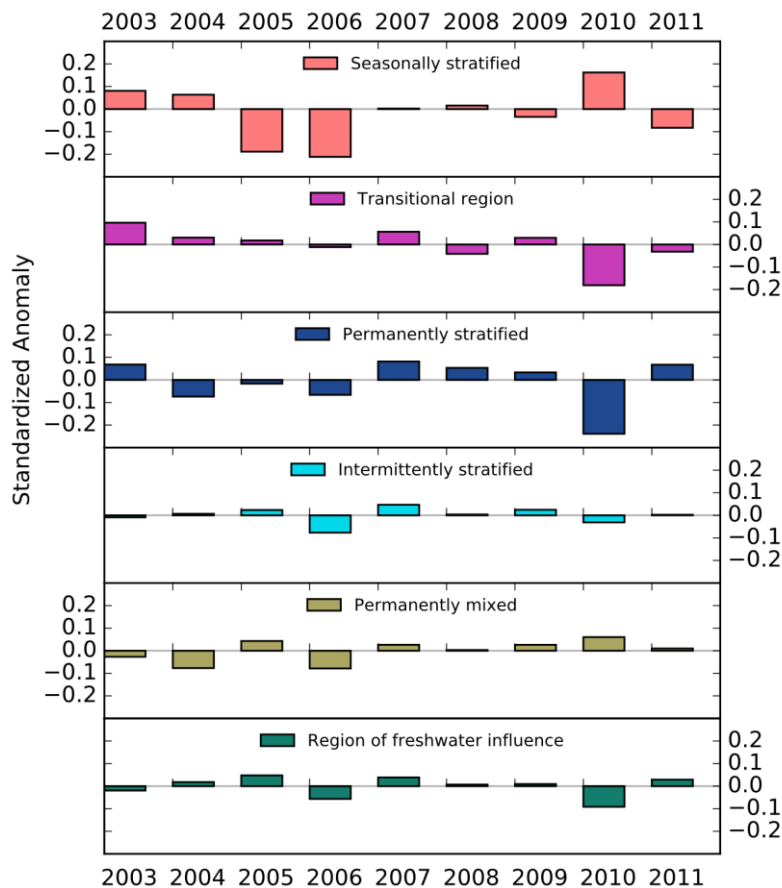
Figure 17: Standardized anomalies of the daily average production values per year (gC/m2/day). Calculation of standardized anomaly is shown in the methods section.

3.3.2 *Monthly averaged composites of North Sea primary production*
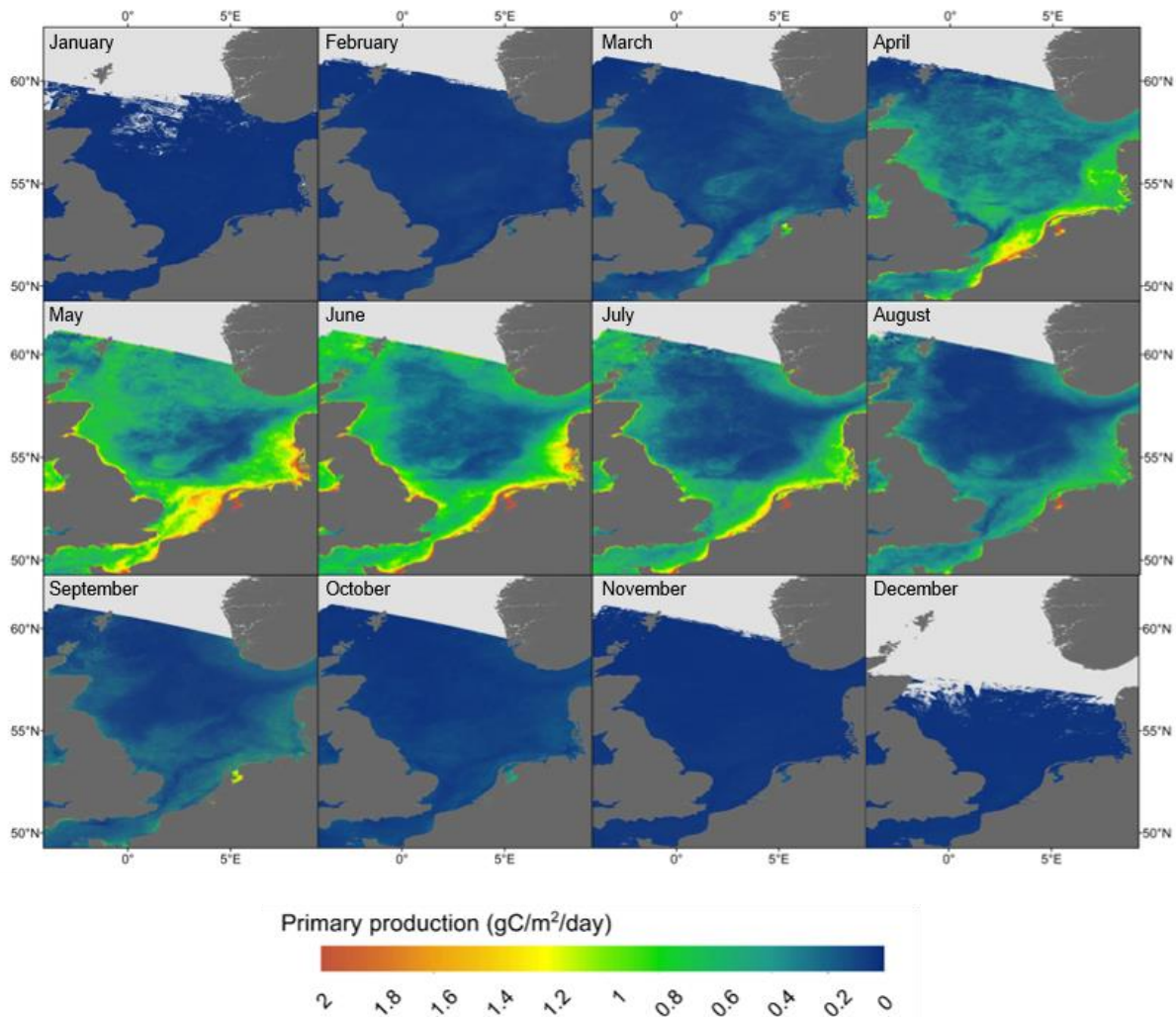
Figure 18 illustrates the monthly composite images of primary production in the North Sea averaged over the years 2002-2012. It can be generally observed that for primary production is generally the lowest between October to February. In March, some regions start to exhibit increases in primary production, especially near the coastal areas around The Netherlands and Belgium, and the relatively shallow Doggerbank area. For the central to northern parts of the North Sea, primary production reaches its peak around March and April before generally declining in the following months. The coastal areas, especially the region of freshwater influence, appears to have persisting conditions of high primary productivity even up till July, before declining from August onwards. In general, higher primary production values are observed near coastal areas, and more so in the southern part of the North Sea than the north. Visual analysis shows that peak production values typically occur between April to July before decreasing again. It can even be observed that the IJsselmeer in
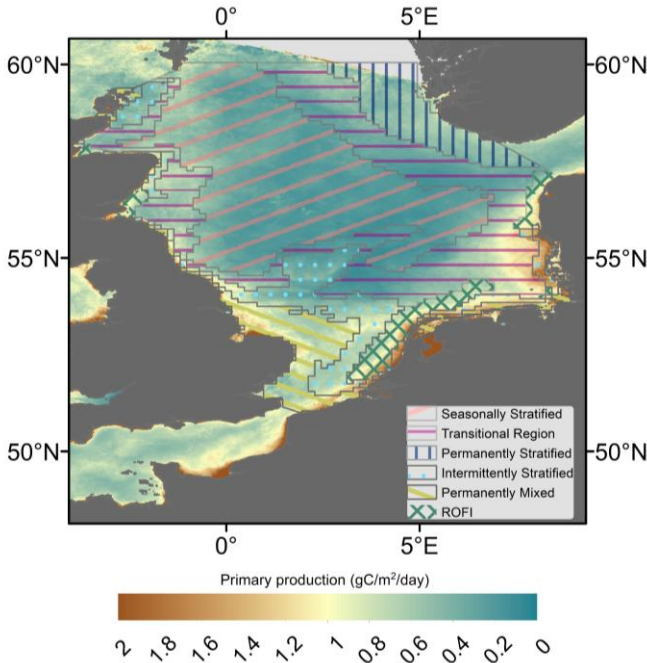
Figure 19: Hydrodynamic regions overlaying the monthly composite image of June.

the northern part of The Netherlands shows much higher primary production values than the rest of the North Sea between March to October.

The spatial patterns of primary production correspond well with the locations of the hydrodynamic regions. This is illustrated in further detail with the composite image of the overall averaged month of June overlain by the hydrodynamic regions, represented by the different patterns in Figure 19. However, as can already be seen in the figure, although the ROFI region reports the highest mean primary production values per square metre on average, some parts of the North Sea with high primary production occurring coincides with other hydrodynamic regions as well i.e. the intermittently stratified region along the east of the Wadden Sea. Therefore, even within hydrodynamic regions, there can be some high level of spatial variability too. The seasonally stratified region can be observed to almost exactly overly the middle of the North Sea, which consistently shows the lowest primary production values even in the monthly composite images in Figure 18.

3.3.3   Phenology – Latitudinal changes and bathymetric depth
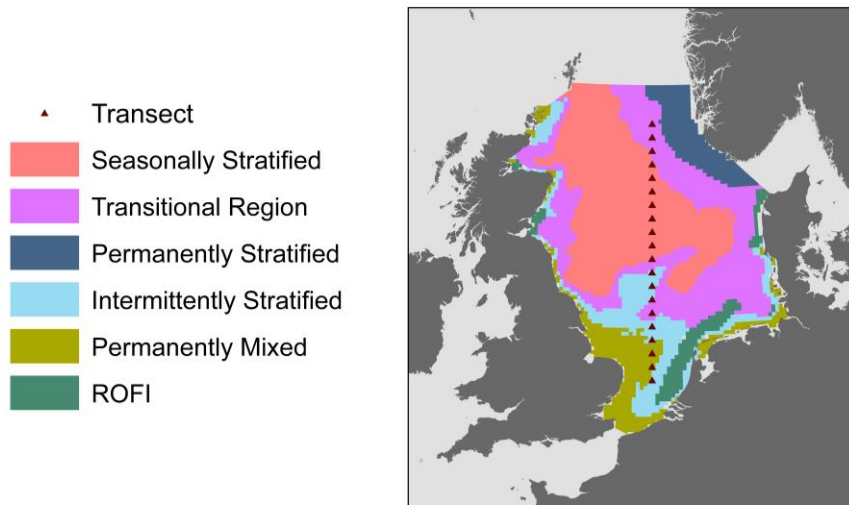
Figure 20: Map of transect used to extract GPP values for phenological analyses

To investigate the phenology of GPP in the North Sea, 20 values were extracted from a North-South transect approximately 0.35° apart from each other (see Figure 20 for location of transect). The transect cuts across 4 different hydrodynamic regions except the permanently stratified region and the ROFI. First, latitudinal variations in primary productivity were plotted in Figure 21, and Figure 22 illustrates primary productivity at variable bathymetric depths, i.e. total depth of a water column.
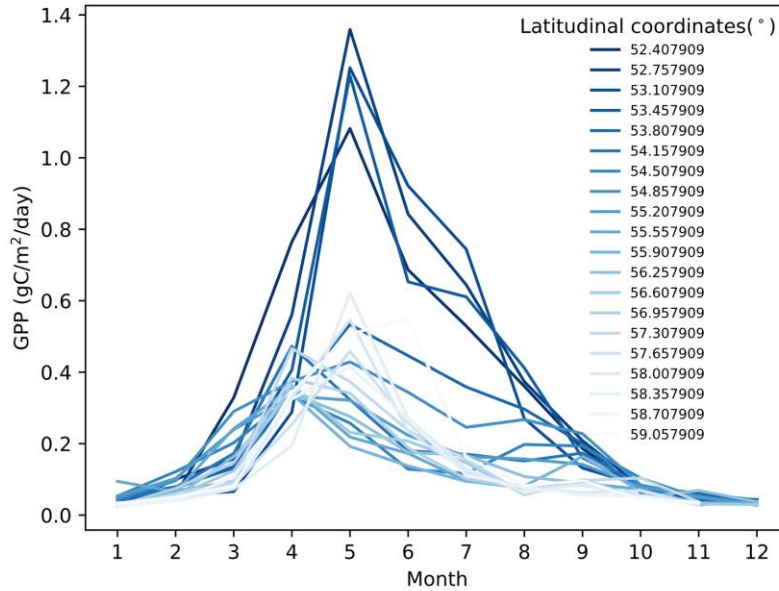
Figure 21: Latitudinal changes in primary productivity in the North Sea across a year. Longitude remained at a constant of 2.978268°W. Dark blue indicates lower latitudes, light blue indicates higher latitudes.
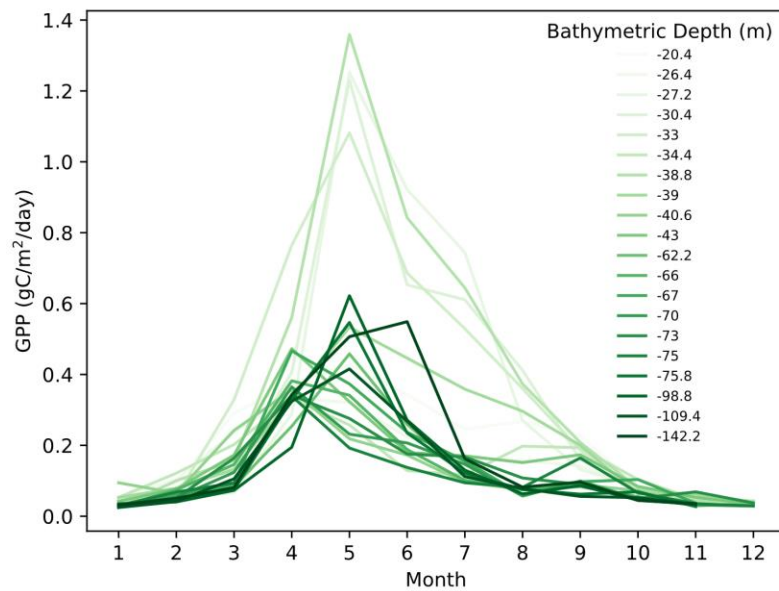
Figure 22: Variation in primary productivity at different bathymetric depths (total depth of water column). Shallow areas are indicated by the light green lines, while deeper parts are indicated in dark green

For Figure 21, it can be observed that the lower latitudes (52°-53°N) dominate the highest primary production values by a factor of approximately 2, compared to the other latitudinal values. Although higher latitudes do have lower primary production values, they are not necessarily the lowest. It can also be observed that lower latitudes have a large, single peak in primary production occurring around May, while some primary production values from the higher latitudes show two peaks in primary production, one around April-May and another in September-October. Sample locations that had these double peaks in primary production also lie within the seasonally stratified region. Furthermore, the highest primary production values come from locations within the permanently mixed region, which also happens to have one of the highest primary production values per square metre per day in the North Sea (see Figure 12). When compared with Figure 22, the highest primary production values also belong to the shallowest bathymetric depths from the transect, though some plots with shallower depths i.e. 20.4m had much lower primary production values than the other shallow depth locations. The transect points with the greatest bathymetric depths have primary production values that peak at an increasingly later part of the year, e.g. line plot of 142.2m bathymetric depth, which has a prolonged bloom season with a peak in June before decreasing and having a small peak in August as well. In addition, the increase in bathymetric depth coincides with the increase in latitude, but this is likely due to the fact that the deepest part of the North Sea is towards the northern part of the basin (see Figure 2).

4 Discussion

4.1 Evaluation of results for station OS9

Table 3: Comparison of the 'a' and 'b' terms across different stations in the Scheldt Estuaries. OS1, OS2, WS1, WS4 data is provided by Kromkamp (unpublished).

Location (station name) / other studies	Reference	Equation $PP = a(BPI) + b$		r^2
		a	b	
Eastern Scheldt (OS1 & OS2)	Gwee (2017)	0.6758	114.6	0.75
Western Scheldt (WS1 & WS4)	Gwee (2017)	0.8305	60.3	0.89
Scheldt (OS1, OS2, WS1, WS4)	Gwee (2017)	0.717	97.1	0.79
North Sea (OS9)	This study	0.721	46.1	0.94
Cole & Cloern (*1987*)*	Cole & Cloern (1987)	0.73	150	0.82
North Sea	Capuzzo et al. (2017)	0.76	45.6	0.86

*For the calculation of the a and b terms, Cole & Cloern calibrated the BPI model based on primary production values derived from 24hr incubations and measured using ^{14}C-labelling method.

The *a* term in the BPI model describes the efficiency of light utilization, while the *b* term acts as a correction factor when estimating primary production. By comparing the *a* terms derived from different regions, we can make inferences about the similarity of the light climate and utilization within the water column of the various areas. A previous study on the Scheldt estuaries included deriving two different *a* and *b* terms for each region (Gwee, 2017) by applying the BPI model from Cole & Cloern (1987). This was also performed on the in-situ water quality parameters in the North Sea by Capuzzo et al. (2017). Table 3 shows the comparison of the *a* and *b* terms from regions and studies, and we can see that although the *a* term for OS1/OS2 and WS1/WS4 were different by approximately 0.16, combining these 4 stations resulted in an *a* value (0.717) that is not too different from the *a* term derived from OS9 (0.721). OS9 is the only station that lies outside of the storm surge barrier, thereby not affected by the limited mixing with the open sea as other stations are. Cole & Cloern (1987) applied the BPI model onto a dataset that included samples from Puget Sound, New York Bight and the San Francisco Bays (North and South). The *a* and *b* terms they obtained are also shown in Table 3. Despite the differences in location, the *a* term that Cole & Cloern derived is remarkably similar to the *a* term achieved for station OS9. Another observation is that the both the *a* and *b* term from Capuzzo et al. (2017) is quite similar to the one derived from station OS9. However, it must be noted that the *a* term that Cole & Cloern derived were based on in-situ measurements of primary production made from 24hr incubation experiments and measured using the ^{14}C-labelling method. While the data from the Oosterschelde and Westerschelde stations were acquired from similar experiments, the incubation period was only 2hr instead. Cole & Cloern's BPI model was, therefore, measuring net photic zone production, as opposed to Kromkamp & Peene (2005), where the 2hr

incubation periods were attempting to measure gross primary production instead. Yet, Capuzzo et al. (2017) incubated the samples for only 1-hr, and were attempting to measure gross primary production as well. The question therefore remains whether *a* and *b* terms used in this project have been suitable in deriving reasonable estimates of gross primary production alone. As I will later discuss with the results of the primary production estimates, this will remain a point of contention.

As gross primary production does not take respiration into account, GPP values will be higher than NPP values, and can range between 1.2 to 7 times the net primary production values (Milligan et al., 2015). Hence, the *a* values derived from the BPI model for the Oosterschelde and Westerschelde stations will likely be lower if incubation experiments were longer and net primary production was measured instead. The exact difference in the *a* and *b* terms between the different locations found in literature is not known unless similar incubation periods are used in these experiments. Yet, it has been found that the ^{14}C method can be unreliable in measuring gross primary production even in short incubation periods due to a range of reasons including metabolic requirements of phytoplankton, which differs across species (Halsey et al., 2015). Another question remains if *a* values are consistent through time and space. Since production data was retrieved from a single location, there is still a need to test for spatial heterogeneity. Additionally, OS9 sample points were from a 2-year sampling period between 2007-2008. Kimmere et al. (2012) studied primary production in the San Francisco estuary and found that the *a* value changed from approximately 0.7 to 0.4 between 1989 and 2003. The period in which North Sea images were analysed may be too short to examine temporal changes in the '*a*' term as well, and the timing of the OS9 data sampling occurred around the middle of the period of analysis. To properly test the temporal change in *a*, more data is needed from different parts of the North Sea and from different years than the available OS9 samples. Although there were only 8 data points from OS9 to calculate the BPI composite parameters, these samples were taken from different parts of the year, including both the winter and spring-summer seasons. This is important as samples coming from similar seasons alone may not fully explain the variations in primary production since photosynthesis rates are variable throughout time and space (Heip et al., 1995).

The availability of satellite images did not always coincide with the dates of the sampling points. Of the 8 sampling dates, only images for 4 dates contained pixel values for OS9. To further increase the number of data points for validation purposes, composite images of 3 days (±1 day including sampling date), yet, only images for 5 composited dates contained pixel values for OS9. Although the *r²* values may not necessarily be meaningful, the range of values extracted and compared against will be more useful. As observed, the range of chl-a values from satellite imagery appear to be larger than the measured chl-a values, with an average of up to 2.7 times more than measured values while K_d and SPM have a range of underestimated values. As E_o values are from the NCEP Reanalysis 2 model, daily values

are available, which explains why it is the only parameter in which all 8 data points could be validated. The p-value was tested and the regression coefficient of 0.67 is moderately significant. The E_o values obtained have a source of error originating from the number of daylength hours. As previously mentioned in the Methods section (not mentioned yet, insert section reference number here later), the average mid-point of the North Sea was taken as input coordinates for the calculation of daylength hours, resulting in a maximum error of ±0.0015*PP. In addition to this source of error, E_o values are underestimated by approximately 0.67 of the measured values. As OS9 is a station that lies south of the mid-point, it has a lower latitude than the mid-point. If Eo values are affected by the difference in daylength hours, this would theoretically result in a slight overestimation of the values from the summer season, and an underestimation if it was from the autumn-winter season.

Results of the primary production comparison between measured and satellite-derived values (Figure 8) poses a level of uncertainty - the lack of data availability makes it difficult to achieve a reliable validation and hence, appropriate calibration to constrain the model if needed. This is resolved due to the validation of satellite-retrieved parameters using the Rijkswaterstaat station data, which will be elaborated on in the following section. Despite this issue, the overestimation observed may be a significant result. Overestimation was also observed in a pilot study on modelling primary production in the Scheldt estuary on satellite images using the same BPI model (Gwee, 2017). The overestimation was by a factor of approximately 3 times for the Oosterschelde, which has clearer waters and less light dependent than the Westerschelde, which had an overestimation of approximately 2 times the measured values. However, considering that there are insufficient data points to deduce an appropriate conclusion about how satellite-derived parameters perform, the next section, which includes validation of parameters using the extensive Rijkswaterstaat datasets, will help provide an idea on how to interpret the validation results of OS9.

4.2 Evaluation of satellite-retrieved parameters for the Rijkswaterstaat stations

Comparison of water quality parameters from measured and satellite-retrieved values yielded reasonable regressions. Though the datasets were retrieved from the Dutch part of the North Sea, the locations of the Rijkswaterstaat sample points are situated in at least 3 different hydrodynamic regions: the ROFI, intermittently stratified and seasonally stratified regions. Considering these points were from different hydrodynamic regions, the regression coefficients and corresponding *p*-values show that significantly reasonable and reliable estimates of these water quality parameters can be retrieved for the North Sea thus far. However, light attenuation K_d and SPM are underestimated by an approximate factor of 2. Chlorophyll-a match-ups show more scatter than the other water quality parameters, yet, it also has the most number of match-ups than light attenuation or SPM. This is primarily due to the availability of data, as the Rijkswaterstaat datasets contained much more chlorophyll-a measurements than the other parameters.

Interestingly, the regression plots of the Rijkswaterstaat datasets versus satellite-derived values show that chl-a values are almost on a 1:1 scale for the Dutch part of the North Sea, unlike in station OS9 where satellite-derived chl-a values are almost twice the measured values. While this is the case for chl-a, the light attenuation coefficient and SPM values are also underestimated by a factor of 2 in comparison with the Rijkswaterstaat datasets, though not on the same magnitude as observed in OS9. For OS9, K_d values are almost underestimated by 5 times the amount, while SPM values are underestimated by approximately 3 times the amount. This does show that sufficient data points are needed to draw significant correlations and conclusions about the validation of the water quality parameter algorithm used on MERIS images.

Results of the distance from coast versus parameter values for both measured (Rijkswaterstaat) and satellite-derived values indicate an overall general trend of decreasing values as the points progress further offshore. For chlorophyll-a, this is a typical trend observed in other environments as well. An example includes the observation of RuBisCO gene expression levels varying with respect to distance from shore from the Tampa Bay estuary to the Gulf of Mexico. Results showed that the total photosynthetic biomass generally showed a decreasing trend from nearshore (0km) to offshore waters (235km) (Paul & Pichard, 1998). However, the cause of such a trend may vary across systems. An inter-comparison between measured and modelled values of nutrients and phytoplankton biomass was conducted by de Vries et al. (1998). Results showed that nutrient concentrations, including Dissolved Inorganic Phosphorus (DIP) and Dissolved Inorganic Nitrogen (DIN), decreased further offshore the Dutch Coast. In addition, the N:P ratio changes from being more phosphorus limiting in the nearshore environments up to

approximately 20km, before becoming more nitrogen limiting after 50km onwards. Phytoplankton biomass, measured as chlorophyll, also showed decreasing trends from nearshore to offshore environments, though the largest decrease occurs between 0-5km off the coast. The decreasing trend from nearshore to offshore environments coinciding with changes in nutrient concentrations is not limited to the Dutch part of the North Sea – this trend is also observed elsewhere i.e. UK coast, German Bight, Northern Central North Sea etc. (de Vries et al., 1998), where annual primary production values plotted against DIN concentrations show increasing production values when DIN concentrations increase as well. In the English Channel (southern part of the North Sea), model results show that the spatial gradient of chlorophyll concentrations from nearshore to offshore may be correlated to salinity, as a result of the influence of freshwater and the high nutrient loading associated with riverine input (Desmit et al., 2015). It is likely that the reason why decreasing chlorophyll-a trends are found with respect to distance offshore is related to nutrient loading associated with freshwater discharges. Yet, the decrease in chlorophyll-a can also be explained by a decrease in cellular chlorophyll-a content when met with a nutrient limitation or increasing light availability in the aquatic environment (Flynn, 2001). For SPM, the behaviour of decreasing values with increasing distance from shore has also been observed in other studies of the Dutch coast, where high SPM values were found at nearshore or shallow areas, and low SPM values were found in deeper offshore zones (Eleveld & van der Woerd, 2006). Like chlorophyll-a, this is correlated with freshwater input which directly affects SPM transport (de Kok, 2002).

4.3 Primary production in the North Sea

The annual variability in primary production across all hydrodynamic regions (Figure 12) i.e. low primary production during winter months and peak primary production during spring-summer months is in agreement with typical trends for temperate regions (Uitz et al., 2010). The seasonal variability of light due to the latitudinal location means that summer experiences the longest days while winter experiences the shortest days. Therefore, daily surface irradiance is directly correlated to the day of the year. Since primary production is a function of light, it is no surprise that the increase in primary production typically coincides with increases in daylength, which mainly explains why all hydrodynamic regions experience the large increases or decreases in primary production together. Additionally, the reason why the Region of Freshwater Influence experiences one of the highest primary production rates can be explained by the fact that it has the highest influence of freshwater input. Freshwater discharge contains high nutrient concentrations (Desmit et al, 2015), and since nutrient can also be a limiting factor for primary production, this can contribute to high primary production values. Stratified regions do not typically show high primary production

values, and this is due to the stratification regime of the water column preventing mixing, hence restricting a source of nutrients for use in primary production (Behrenfeld et al., 2006). Furthermore, it is observed that stratified areas in the North Sea appear to have a characteristic spring bloom, which is explained in the next paragraph.

Timing of blooms in the different hydrodynamic regions

The timing of the peaks has several explanations for each hydrodynamic region. As mentioned earlier, stratified areas in the North Sea appear to be characterized by a spring bloom. This can, in fact, be explained by Sverdrup's 'Critical Depth' theory. The critical depth refers to the depth at which total production is equals to the total amount of respiration occurring. The Critical Depth theory states that the spring bloom is initiated due to increasing thermal stratification. This causes the mixed layer to become shallower, resulting in the mixed layer depth to be above the critical depth. When this occurs, net phytoplankton growth occurs, thus contributing to a bloom. The Critical Depth theory particularly applies to stratified waters, therefore, does not necessarily apply to coastal and shallow shelf environments where water density may be more strongly influenced by salinity instead (Lucas et al., 1998). In the case of satellite-derived primary production for the North Sea, the intermittently stratified, seasonally stratified and permanently stratified regions often also experience double peaks in primary production, while the ROFI and permanently mixed regions appear to experience a large distinct peak in primary production typically around July or July, and very rarely experience a second bloom in primary production. Van Leeuwen et al. also argues that stratified regions often experience two blooms in primary production due to changes in the mixing regime of a region. The first bloom is therefore typically a spring bloom initiated due to high nutrient concentrations, followed by a second bloom occurring after changes in mixing that allows phytoplankton to access nutrient-rich waters that was previously unavailable due to stratification (2013). In many cases, the timing of the peaks also coincides with trends in phytoplankton dynamics throughout the year. Van Leeuwen et al. (2015) showed the results of modelled annual mean phytoplankton dynamics for all hydrodynamic regions except the transitional region. The double bloom observed to occur in the seasonally stratified region agrees very well with

Figure 23: Results of the biological model from van Leeuwen et al. (2015).

phytoplankton dynamics in the North Sea. The initial spring bloom occurring around April/May coincides with a sharp increase in diatom biomass, while the autumn bloom that occurs around September/October is shown to coincide with an increase in dinoflagellates for that region. At least for the case of the seasonally stratified region, the double peaks observed in the results of modelling primary production in the North Sea agrees with the biological model results of van Leeuwen et al. (2015). Yet, in the case of the ROFI, this is characterized by two very large distinct peaks in phytoplankton biomass. This is shown in Figure 23, which is taken directly from van Leeuwen et al. (2015). In the biological model, the first peak is largely made up of diatoms, and occurs around April. Following the decrease in diatom biomass, the phaeocystis colonies start to increase around the same order of magnitude as diatoms and peaks in June. When directly compared to trends in primary production of the ROFI in Figure 12, primary production trends for the ROFI in 2005, 2010-2011 shows a somewhat prolonged peak in primary production spanning from around April-July, and these trends agree well with the results of the phytoplankton biomass model of van Leeuwen et al. However, as this is not always observed in the data throughout the entire period, the results are a little more difficult to reconcile with the results of van Leeuwen et al.'s paper (2015). There are many factors that could affect the reason why we do not observe distinct double peaks, and these include the fact that diatom abundance is limited by silica, which can explain the timing of the peaks. If there is silica limitation, regions dominated by diatoms may not always experience spring blooms of the same magnitude every year, and instead, the contribution of primary production may be dominated by phaeocystis due to the prolonged period of abundance that can be observed in Figure 23. Another reason that may explain the difficulties in comparing between primary production results in this project and van Leeuwen et al.'s results is that the biological model of van Leeuwen et al. averages phytoplankton dynamics between the years 1958-2008. This may present itself as a problem when comparing results as literature has shown that the North Sea experienced a significant regime shift during the 1980s (McQuatters-Gollop et al., 2007; Weijerman et al., 2005). Regime shifts are defined here as "*changes in species abundance, community composition and trophic organization occurring at regional or greater spatial scales either in response to an external physical or anthropogenic driver*" (Kraberg et al., 2011). The regime shift experienced in the North Sea during the 1980s was characterized by a significant increase in biomass (chlorophyll-a). The regime shift was shown to have been caused by a combination of climatic factors such as changes in Sea Surface Temperature (SST), but most importantly, it was also shown that changes in nutrient loads were not the cause of the regime shift. Overall, however, it can be observed that the primary production results derived from satellite imagery agrees well with expected results based on the stratification regime of the various regions in the North Sea. The monthly composite images also accurately reflect the timing of the peaks. For example, as mentioned earlier, stratified regions tend to experience early spring blooms. This is evident even from the month of March, where pixel values representing primary production start to increase in both the permanently stratified areas

(eastern North Sea) and the seasonally stratified region (middle to northern part of the North Sea).

Anomalous primary production results from 2006 & 2010
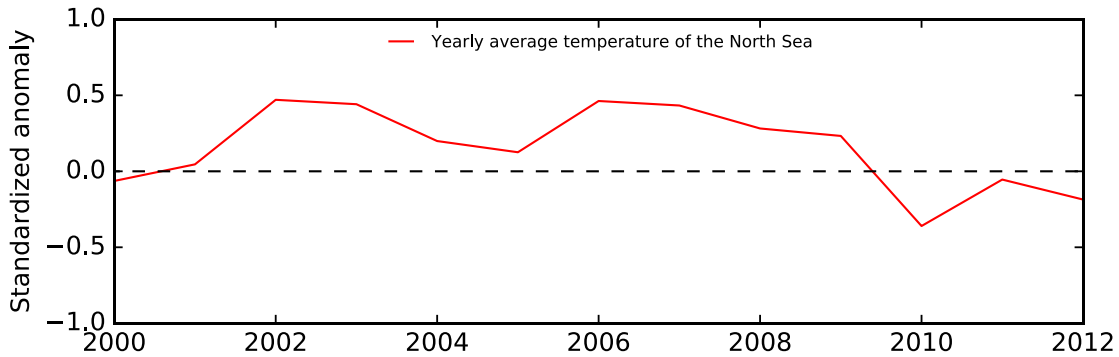
Figure 24: Yearly average sea surface temperature of the North Sea as a standardized anomaly plot between the years 2000-2012. Data taken from the European Environmental Agency (EEA).
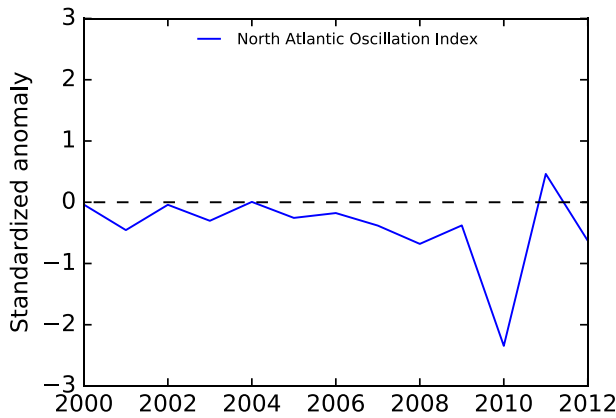
Figure 26: North Atlantic Oscillation index based on pressure differences between Iceland and Gibraltar. Data taken from KNMI
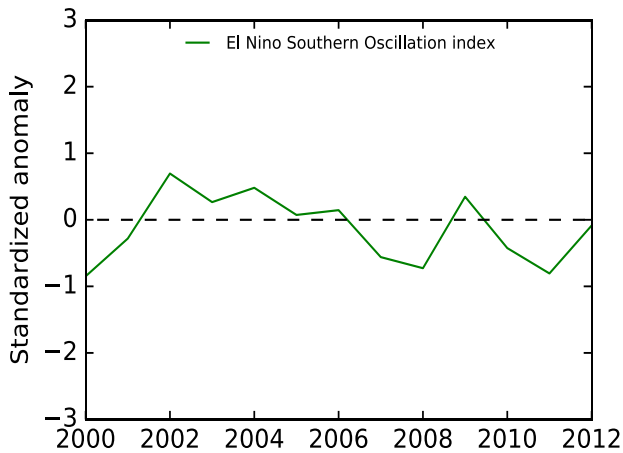
Figure 25: El Nino Souther Oscillation index based on NINO3.4. Data taken from KNMI

The North Sea experienced anomalous primary production results in the years 2006 and 2010. The standardized anomaly plot from Figure 17 showed that in 2006, all regions experienced a negative anomaly index for daily mean primary production per square meter, although this was almost negligible for the transitional region. Looking at the annual primary production budget of the North Sea in Figure 16, the decrease in mean primary production values resulted in an overall decrease in the budget of the North Sea by approximately 2.83 (10^{12})gC/year. Although the North Sea recovered abundantly the following year by 4.726 (10^{12})gC/year, this still presented itself as an anomalous result in the data. Yearly averaged SST records of the North Sea presented as standardized anomalies in Figure 24 show that 2006 was a warmer year than 2005. A study by Boitsov et al. (2012) also showed that the Barents Sea, a regional sea north of the North Sea, faced anomalously high air and sea surface temperatures, and recorded the highest

values in a 110-year observational maximum. Due to such high temperatures, it is possible that primary production was reduced due to thermal stratification. This occurs when temperatures increase, resulting in a shallower mixing depth that physically restraints access to nutrient richer waters, thereby rendering the water layer nutrient limited (Sarmiento et al., 2004). This idea, however, is a contested paradigm for now. Although primary productivity has been thought to decrease due to warming, it has been shown that oceanic productivity is affected by a host of variables not limited to temperature changes, and in fact, shows poor correlations with changes in temperature (Lozier et al., 2011). To assess if other climatological variables may have also been responsible for the decrease in primary production, the results are also compared to the North Atlantic Oscillation (NAO) index and the El Nino Southern Oscillation (ENSO) index from NINO3.4. The NAO is defined as a change in surface pressure caused by oscillations of air mass between the Arctic and subtropical Atlantic (Hurrell, 2001). This climate phenomenon occurs on a decadal-scale. During a negative NAO index, some of the climatic changes that may affect the North Sea are changes in precipitation. In 2006, the NAO index was negative (see Figure 26), however, this was a value that hovered around the average index between 2000-2006. Therefore, even if the NAO had a negative index, it was not a particularly strong one compared to other years i.e. 2010. The ENSO index also features a near-zero standard anomaly value for the year 2006 in Figure 25. This likely indicates that when considering regional interannual or decadal variability, the decrease in primary production may have been attributed to temperature changes rather than climatic oscillations in the North Sea. Additionally, the primary production model based on in-situ measured parameters from Capuzzo et al. (2017) also showed lower GPP values for 2006 and attributed it to warmer than average SST as well. This warmer than average SST is likely explained by the fact that there was an intrusion of warm Atlantic Water 350km north of the usual position (Walczowski et al., 2012). 2006 also saw a dramatic decrease in sea ice cover along with a thinning of Arctic sea ice related to the intrusion of the warm AW into the Nordic Seas (Alexeev et al., 2017).

2010, on the other hand, saw an anomalously negative index for the NAO and a negative index for the ENSO. Temperature records show that 2010 had a lower than average sea surface temperatures. However, the main difference between primary production results from 2006 and 2010 is that most regions saw a reduction in primary production in 2006, yet, 2010 saw a plethora of mixed results from the different hydrodynamic regions. For example, the permanently stratified region saw the greatest reduction in annual mean primary production values per square meter, while the seasonally stratified region experienced an increase in annual mean primary production values per square meter. Some of the reasons why several hydrodynamic regions saw a decrease in primary production values is due to the fact that the North Atlantic Oscillation influences the amount of freshwater inflow into the North Sea (Vermaat et al., 2008). The positive linear relationship means that a negative NAO index usually results in a lower total river input, while a positive NAO index usually

results in a higher total river input into the North Sea. On one hand, reduced freshwater discharge will result in decreased nutrient loads into the North Sea. Yet another potential cause for reduced primary productivity is that high SPM concentrations have been found to coincide with low river input (Fettweis et al., 2010). An increase in SPM concentrations potentially leads a decrease in water clarity, thereby reducing light availability and contributing to a reduction in primary production. Primary production results from regions that classify as near-coastal environments such as the ROFI or permanently mixed region are therefore likely to be correlated with fluxes in riverine discharge. However, areas like the permanently mixed region and seasonally stratified region experienced an increase in primary production instead during 2010. This cannot be explained alone by changes in freshwater input into the North Sea. For the permanently mixed region, the NAO index correlates positively with the degree of vertical mixing. A negative index, like in 2010, will therefore normally correspond with less vertical mixing. As the permanently mixed region is predominantly the southern part of the North Sea, this is an area which experiences very high SPM concentrations due to the East Anglian Plume (Capuzzo et al., 2015). There is a possibility, however, that the negative NAO index contributed to a decrease in vertical mixing, which may have increased light availability of the region and thus, resulted in increased primary production occurring in 2010 for the permanently mixed region. Additionally, lower SSTs would hypothetically result in a decrease in stratification, allowing the mixing layer to be deeper and therefore, physically unrestricting access to nutrients for phytoplankton. A variety of reasons may explain the primary production results for the different hydrodynamic regions, however, despite the large changes in primary production values, this had not impacted the total annual area-integrated primary production budget of the North Sea and instead, remained constant. This brings us to the next point in the discussion, where despite the large fluctuations in average primary production values per square meter, the total area of the hydrodynamic region matters far more in terms of contributing to the annual primary production budget of the North Sea.

Contribution of the hydrodynamic regions to the annual primary production budget

Table 4: Tabulated area of each hydrodynamic region. Calculated using ArcGIS 10.5 and the region was clipped according to IHOP's definition of the North Sea. The total area calculated here is different than the reported 750,000km2 as the hydrodynamic regions were calculated according to the cut-off area from van Leeuwen's shapefiles. Coastal areas such as inlets and estuaries were also excluded from their shapefiles, explaining the difference in area.

Hydrodynamic region	Area (km^2)
Seasonally Stratified	$1.71 * 10^5$
Transitional region (East and West)	$1.36 * 10^5$
Permanently Stratified	$3.34 * 10^4$
Intermittently Stratified	$5.93 * 10^4$
Permanently Mixed	$4.72 * 10^4$
Region Of Freshwater Influence (ROFI)	$2.27 * 10^4$
Total area	$4.7 * 10^5$

Table 4 shows the total surface area of each hydrodynamic region, of which the seasonally stratified region has the largest surface area, while the ROFI has the smallest surface area. When compared directly with the annual contribution of primary production to the budget of the North Sea for each hydrodynamic region, the hydrodynamic regions in descending order of the largest to smallest contributor is exactly the same as the descending order for largest to smallest areas. Therefore, despite large interannual variations in a region i.e. ROFI, this has little to no impact on the overall contribution to the annual North Sea primary production budget. This explains why in 2010, despite 4 out of 6 regions experiencing a decrease in annual primary production per square metre, the increase in the seasonally stratified region helped offset the decrease in primary production values from those regions, resulting in little to no change in the overall annual primary production budget for the entire North Sea. The implication for this, however, is that changes in primary production for the largest regions i.e. seasonally stratified and transitional region, would result in significant changes to the primary production budget of the North Sea. Furthermore, the North Atlantic Oscillation affects the North Sea in different ways and brings about different responses in primary production values for all the different hydrodynamic regions, meaning that more research is required to fully understand the effects of the NAO on primary production in the North Sea (Deser et al., 2016). Additionally, the period of study for this project is too short to deduce the effects of NAO on North Sea primary production as only a single negative NAO index event occurred. Furthermore, the negative NAO index occurred at the same time as an El Nino event. Yet, the full extent of the effects of the ENSO on the North Sea climate are not yet predictable due to the varying responses of the climate to each individual ENSO event (Brönnimann, S., 2007), making it difficult to quantify and predict future changes. Much like the ENSO, the effects of NAO are not always the same for every event, and therefore might affect the North Sea differently in every occurrence (Deser et al., 2016).

Annual budget and changes in long-term trend of North Sea: a comparison with literature

In this project, the total annual depth-integrated primary production budget of the North Sea was calculated and had an average value of 43.9 (10^{12}) gC/year, ranging between 40.9-44.8 (10^{12}) gC/year. This value was averaged over the years 2003-2011, as 2002 and 2012 were excluded due to insufficient summer months available, as most of the primary production in the year occurs between the April-September months. A study by Capuzzo et al. in 2017 used a similar model by Cole & Cloern (1987) but modelled primary production using in-situ measured parameter values instead. For the period between 1988-2013, GPP was modelled and the results showed a statistically significant decrease in primary production values in the North Sea for each hydrodynamic region. On average, their average GPP values for the period modelled was 97.3 ± 6.9 (10^{12}) gC/year. From 2000-2013, GPP ranged between 50-100 (10^{12}) gC/year for the North Sea. A quick comparison reveals that Capuzzo et al.'s values are estimated to be twice as much as the results derived from this project. Using the annual primary production values per square meter per year, the values ranged between approximately 60-160 gC/m^2/year. A comparison with an older modelling study by Varela et al. (1995) and Moll (1997) showed that the range of annual primary production values per square meter per year were in the range of 200-400 gC/m^2/yr and 40-370 gC/m^2/yr respectively. Modelling primary production using satellite-derived estimates of the individual parameters shows that the results may be underestimating the budget of the North Sea's primary production, when compared to literature. Capuzzo et al.'s (2017) study validated the primary production model using GPP values derived from 1-hour incubations, compared to the 2-hour incubation period used in the GPP values of the OS9 data in this project. A study by Macedo et al. (2002) shows that incubation periods matter, even if it differs by an hour. The table below shows the results of the experiment Macedo et al. conducted, which features three different experiments and GPP calculated from the Photosynthesis-Irradiance (P-I) curves.

Table 5: Daily gross primary production (not depth-integrated) from Macedo et al. (2002) featuring different incubation periods and the effects on GPP values

Experiment	Incubation period (minutes)	GPP (mg C/m^3/day)
I	45	358.7
	120	223.7
II	45	67.8
	120	50.4
III	30	464.8
	180	406.6

Results show that a difference between 45 minutes and 2hr incubation periods in GPP values amounted to around 135 mgC/m^3/day. Furthermore, in Experiment I, incubation period of 2 hours showed a lower GPP value than an incubation period of 45 minutes. This already suggests that some respiration had already occurred when incubated for two hours. This is shown in both Experiment I and II, although Experiment III also shows the decrease, the incubation period was for 3 hours. Macedo et al. (2002) also argue that the incubation period

required to measure GPP or NPP is highly dependent on the environment and the light climate of the water, in addition to the acclimation of the various phytoplankton groups (2002). Therefore, it is possible that instead of featuring underestimations of Gross Primary Production values, the results of this project showed, to a small extent, Net Primary Production values. This may then explain why when compared to the GPP values of other studies of the North Sea, the results of this project had consistently lower values than published literature. A consensus for incubation periods needs to be reached in research separately for GPP and NPP measurements in order to be able to make more useful comparisons with literature studies. It is difficult to assess which time period is suitable for measuring GPP as this also depends on species composition, light utilization and other environmental factors.

The slight increase in slope of the annual primary production budget of the North Sea had a p-value of more than 0.05. This means that the slight increasing trend is insignificant for the North Sea but does not necessarily discount other possibilities. A major challenge is that the primary production in the North Sea was only modelled for a decade, which may be insufficient in determining long-term changes to primary production. Some of the most recent publications feature significant results pointing towards decreasing water clarity (Capuzzo et al., 2015) and decreasing primary production for the North Sea (Capuzzo et al., 2017). As mentioned in the introduction, changes in primary production will be a major concern for the North Sea due to large implications on fishery stocks, water quality and the carbon budget, amongst others. In 2007, McQuatters-Gollop et al. proposed that the North Sea was experiencing increasing water clarity, potentially contributing to an increase in primary production due to increasing light availability. The increasing light availability was proposed to potentially contribute to a regime shift in the North Sea, allowing phytoplankton to become more effective at utilizing lower concentrations of nutrients. However, Capuzzo et al.'s (2015) study on water clarity showed a decrease in long-term measurements of Secchi depth (Z_{sd}), with a 25-75% decrease from the pre-1950 to post-1950 period. The extent of decrease also depends on the different regions and seasons in the North Sea. Another study by Dupont & Aksnes (2013) also showed shoaling rates in Z_{sd} of 1.8 ± 0.3m for shallow waters and 5.2 ± 0.9m for areas with depths greater than 100m. In contrast to McQuatters-Gollop et al.'s study, Capuzzo et al. (2015) hypothesized that climate change and anthropogenic impacts on seabed structures due to fishing have resulted in an increase in SPM concentrations, thus changing the light climate of the water. Therefore, Capuzzo et al.'s (2015) results directly conflict the results of McQuatters-Gollop et al. (2007). Although the method used by McQuatters-Gollop et al. measured phytoplankton biomass using a plankton recorder towed behind ships-of-opportunity and assessing the 'greeness' index of the net. This method is questionable as it is not a direct, quantitative measurement of phytoplankton biomass. Besides this fact, this study is not the only conflicting result from scientific literature. Laufkötter et al. published a global model that showed increase in NPP values between 1960-2006 for the North Sea (2013). They also showed that the population dynamics of the various phytoplankton groups changed for the North Sea, with diatoms increasing by more than 50% in contributing to NPP for the North Sea. Laufkötter et al.

proposed that stronger winds enhance vertical mixing, allowing increase in nutrient access for phytoplankton. On the other hand, Capuzzo et al. (2015) argue that an increase in 'storminess' for the North Sea would resuspend fine matter and result in decreasing water clarity. In contrast with Laufkötter et al.'s study, a model by Holt et al. (2015) predicts an overall net decrease in primary production rates by the end of the century under the business-as-usual scenario. It is therefore clear that the effects of climate change on primary production is not yet fully understood for the North Sea, let alone taking into account the effects of regime shifts on the North Sea ecosystem. McQuatters-Gollop et al. (2007) also argue that a regime shift is more likely to occur in the event of ecosystem stress. If, for example, under the stress of ocean acidification and warming, diatoms would dominate the phytoplankton population of the North Sea, a regime shift would suggest that despite the calcification pressure as a result of increasingly acidic oceans, diatoms, which are unaffected by the calcification pressure due to their silicate frustules, have been shown to adapt due to a membrane protein that allows them to survive under a range of stressful conditions such as nitrogen starvation, darkness, light inhibition and iron limitation (Ashworth et al., 2016). More important, they were found to easily adapt under carbon limitation and elevated CO_2 concentrations, showing a high degree of adaptation and niche broadening under the various types of ecosystem stresses. Therefore, a regime shift marked by dramatic changes in primary production will not be necessarily telling of the overall trends in the North Sea. Thus, a proposed method of estimating overall trends in primary production in the North Sea is to conduct trend regressions on various time periods of primary production in the North Sea, separated by the regime shifts that the region experiences. This may give a better overview of shifts in primary production trends as opposed to assuming phytoplankton dynamics remain the same throughout the years. This method of analysis may also help provide a clearer picture on how changing phytoplankton dynamics affects the primary production budget of the North Sea. An example of this being done is by Tiselius et al. (2016), which features long-term time series of primary production trends in the Gullmar Fjord, Sweden (far eastern part of the North Sea). Regime shifts were marked out in the time-series and linear regression analysis was performed on each individual period. Results even showed a regime shift occurring as recently as 2010. Based on Tiselius et al.'s results, at least more than 4 regimes could be detected between 1985-2012. This period of analysis also coincides with the period of analysis that Capuzzo et al. (2017) undertook for estimating GPP of the North Sea. However, since Tiselius et al.'s study only covers one station from the permanently stratified region of the North Sea, it is still not indicative of overall trends in primary production for the North Sea.

Lastly, an issue encountered is that the surface chlorophyll concentrations of the satellite-derived estimates are assumed to be representative of the water column. van Leeuwen et al. (2013), however, found that the deep chlorophyll maxima alone has the potential to contribute up to 30% of annual NPP values. As the deep chlorophyll maxima (DCM) is most often missed by satellite measurements, the contribution to the total NPP budget is therefore not considered (Weston et al., 2005). The DCM is, however, typical of

stratified waters (Latasa et al., 2016). This may suggest that stratified parts of the North Sea are underestimated with respect to primary production, offering another explanation for the underestimation of annual primary production budget values of the North Sea in this project.

Latitudinal and bathymetric depth variations in primary production

In both Figure 21 and Figure 22, the transect points that also lie within the transitional and seasonally stratified region in the North Sea have a spring bloom occurring around April. These points coincide with greater bathymetric depths as well, which are normally associated with increasing stratification due to the physical inability to homogenously mix water throughout such a large water column in a short time. Although the peak values are around $0.4gC/m^2/day$ compared with the highest peak production values in both figures i.e. almost $1.4gC/m^2/day$, they have a distinctly early occurring peak in primary production, followed by an autumn bloom. Early spring blooms can be explained by Sverdrup's critical depth theory, as mentioned earlier in the discussion. This theory is also well exemplified especially since these early spring blooms coincide with larger bathymetric depths as seen in Figure 22. The autumn blooms occur primarily due to the stratification breaking down in the water column, transitioning towards an increasingly homogenous layer (Humphreys et al., 2018). Although this double-peak trend had already been observed in the time-series (see Figure 12), this is illustrated better in these figures.

The latest major peaks in primary production occurring around June for Figure 21 coincide with the locations of the transect points that had the highest latitudinal coordinates. For the Northeast part of the Atlantic, it has been found that higher latitudes tend to have later bloom seasons than lower latitudes (Friedland et al., 2016). This is in part due to the larger effect of seasonality on higher latitudes than lower latitudes. Another interesting observation is that the primary production values belonging to a bathymetric depth of 142.2m in Figure 22 is observed to have a particularly prolonged bloom season between March and July. This also happens to coincide with the northernmost latitudinal point in the transect, which lies within the transitional region. One explanation for prolonged periods of productivity may be due to grazing pressure and diapause in grazers (Friedland et al., 2016). Friedland et al. argue that diapause in grazers is primarily attributed to overwintering, causing grazers to become active at a much later period than the expected bloom peak, thus allowing for a bloom to initiate and prolong compared to other areas (2016).

In summary, the phenological exploration of the dataset highlighted differences in the timing and magnitude of the blooms which could be explained by the latitudinal variations and differences in bathymetric depth of the water column, which are connected to the effect of seasonality and stratification regime of the region.

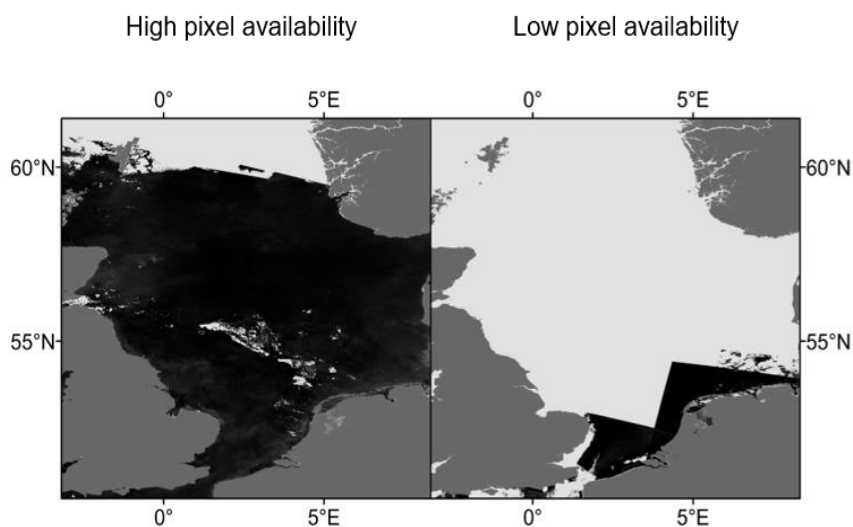# 5 Project challenges & future recommendations

Figure 27: Comparison of pixel availability. [Left]: Self-composited image of June 2007 [Right]: Self-composited image of December, 2003. Light grey indicates no pixel availability.

Although MERIS image products were of sufficiently high resolution to use for analysis, the main challenge faced was deriving monthly composited images of the North Sea. Due to the limitations on computer memory and speed, only images that coincided with the Rijkswaterstaat sampling dates were downloaded. In most cases, the number of images in a month were enough to generate a composite representative of the behaviour of primary production trends during the month. However, this was more often the case for summer months than winter months, as poor weather conditions restricted the frequency of sampling dates for the Rijkswaterstaat datasets. Furthermore, not all water quality parameters were also sampled at the same frequency throughout the years (see appendix for water quality parameter datasets from Rijkswaterstaat), with chlorophyll-a being the most frequently sampled across all stations. This explains the reason why there were more exact point match-ups for chlorophyll-a as opposed to light attenuation coefficient or SPM. Additionally, another reason why pixel availability is often low during winter months is simply due to much higher cloud cover during winter months than summer months, resulting in flagged pixels and contributing to low pixel and/or image availability. Therefore, primary production values generated during the winter months must be treated with caution as pixel availability during the winter months was low, resulting in fewer pixels used to generate zonal averages. Although the model was able to predict annual variations in primary production well, instances such as 2006 January or 2009 December for the permanently stratified region, where a spike in winter primary production values can be observed, should generally be treated as anomalous values due to the fact that the number of pixels used to generate zonal averages is simply not representative enough of the area.

A total of 1403 unique dates were generated from the Rijkswaterstaat datasets between the period that the MERIS sensor was online, and a total of 2742 images of the North Sea were downloaded from CoastColour. The reason why there are more images than unique

dates is due to the sensor taking more than one image of the area in a day i.e. more than one image taken during a single overpass. In some cases, up to 5 images were taken during the overpass over the region within a period of approximately 2 hours (e.g. 19/03/2012). Given sufficient time, another potential area to explore within the dataset is to assess the impact of different viewing angles on the water quality parameter retrieval. Ideally, given sufficient memory and time, daily images should be used for compositing monthly imagery to give a better statistical representation of primary production during the month. The advantage of using such a simple model is that despite the large memory requirements of storing the images, the modelling process was much faster than the process of reprojecting the images onto a coordinate system. The average time taken to apply the model onto each image, calculate a zonal average and generate basic statistics of each region for each month was approximately a week. This means that the time taken to model and generate data is near-instantaneous, opening the possibility to automate this method and retrieve primary production of a satellite on a daily basis. This model, for instance, can be applied onto Sentinel-2 and Sentinel-3's image products, providing potential continuity of primary production modelling through time. As 9 years is still too short a period to deduce statistically significant changes in the North Sea, partly also due to the Nyquist frequency requirements of the North Atlantic Oscillation, the ability to extend the dataset will clarify some of the preliminary observations made in this project. Yet, this should be done only if Level 0 to Level 2 processing for these satellites is similar to the MERIS processing algorithms so that the data can be used for making useful comparisons and providing data continuity throughout the period. The current data products of Sentinel-2 are not suitable for data continuity, even though it is a multi-spectral imaging spectrometer like MERIS. The reason is that the Inherent Optical Properties of the ocean surface for the MERIS products are calculated using a neural network algorithm, of which is not applied to Sentinel-2 processing. Although the individual water quality parameters can be calculated using simple band-ratio algorithms, modelling primary production using the band-ratio results would not be ideal for comparison with MERIS products or provide time-series continuity. Sentinel-3, however, has a dedicated Ocean and Land Colour Instrument (OLCI). Its primary mission is to serve as a continuity of the MERIS mission, which contact was unfortunately lost since April 8th, 2012. The water quality parameters are calculated using a neural network algorithm that is currently using the MERMAID database as a training set, which is similar to MERIS' water quality parameter retrieval process. With a hiatus of approximately 6 years, the launch of Sentinel-3 will allow some level of continuity in monitoring trends in the North Sea with a high level of spatial and temporal resolution. In contrast to MERIS, which has a return time of 15 days, the Sentinel-3 will be able to revisit the exact same location every 3 days at latitudes above 30° N/S and 4 days for equatorial regions (ESA, n.d.), thus providing an even better temporal resolution than MERIS. Yet, Sentinel-3 has different atmospheric correction models applied than MERIS, therefore it is uncertain how comparable the products are until validation is performed on Sentinel-3 products.

The satellite-retrieved water quality parameters in this project primarily used the Level 2 products of MERIS from the CoastColour project. However, water quality parameters like chlorophyll-a and SPM can be derived in ways other than the neural network. The performance of the neural network primarily depends on how much data the network is trained with, which in this case was provided by the MERMAID database. The MERMAID database, however, does not have in-situ measured samples of SPM concentrations higher than 15g/m^3. While most of the North Sea consists of waters close to the Case 1 open-ocean classification, this becomes an issue for turbid coastal environments, which often have SPM concentrations of more than 15g/m^3. Without training on data that encompasses a wider range of SPM values, this may be another explanation for the underestimations observed in SPM and light attenuation K_d. Some of the proposed methods for calculating these water quality parameters include the Gons family of algorithms (Gons et al., 1997; Gons, 1999; Gons et al., 2000 etc.), which involves taking into account chlorophyll absorption bands and a backscattering coefficient to correct for. Other methods available include Wavelength Resolving Model (WRM) from Tilstone et al., (2015) and the band ratio algorithm from Ruddick et al. (2001). In short, many methods have been developed for calculating water quality parameters, with some developed even after the end of the Envisat-MERIS products. The neural network should not be taken solely, as other methods may be more robust such as atmospheric radiative transfer models like HYDROPT (Van Der Woerd & Pasterkamp, 2008).

Primary production was calculated in this project with the BPI model, and as mentioned earlier, this approach works best for nutrient replete systems. By using this model, one of the underlying assumptions is that the entire North Sea is not limited by nutrients, which is not the case in reality. The North Sea has an offshore gradient of nutrients, switching between nitrogen and phosphorus limitation depending on the distance from shore (Burson et al., 2016). This may therefore question the reliability of the model especially in nutrient limiting parts of the North Sea. Another shortcoming of the simple BPI model is that it does not account for phytoplankton species composition in the water. Species composition can have an important role in determining primary production due to different nutrient requirements of the different phytoplankton (Tagliabue et al., 2011) and size of phytoplankton matter sinking out, which influences nutrient cycling (Acevedo-Trejos et al., 2015). Using a simple model with fewer parameters involved therefore discounts other potentially important factors.

6 Conclusion

Although it has not been the first time that primary production has been calculated for ocean waters using satellite remote sensing (e.g. Behrenfeld & Falkowski, 1997b; Balkanski et al., 1999; Hirawake et al., 2012 amongst others), it has been the first time that such a high-resolution time-series of primary production values was generated for the North Sea between the period 2002-2012. Results of this project show that MERIS-derived estimates of chlorophyll-a, light attenuation coefficient and SPM values form good correlations with in-situ measured datasets, although both light attenuation coefficient and SPM values were under-estimated for. As result of the underestimation for light attenuation coefficient, a correction factor was applied onto the primary production model. The long-term time series simulates interannual variability well in the North Sea and shows quite clearly the timing of the peaks for several regions, and even two distinct bloom seasons in the year for some regions, e.g. the seasonally stratified region. The model results also show that it has been able to correctly pick up climatic signals in the primary production values, such as the warm Atlantic Water intrusion of 2006 and a strongly negative NAO index for 2010. The results also show that although regions like the ROFI or permanently mixed areas can reach much higher values in primary production than e.g. the seasonally stratified region, the total area of the hydrodynamic region matters far more for the total North Sea budget as small changes to a large region can have a much bigger impact on the annual primary production budget of the North Sea than smaller areas. This is evident in 2010, where 4 out of 6 regions experienced large decreases in primary production. While the seasonally stratified region saw an increase in primary production values, this was not as dramatic a change in value than e.g. the permanently stratified are for 2010. The increase in the seasonally stratified region alone was able to offset the overall decrease in primary production. Furthermore, this also goes to show that climatic phenomena such as the NAO does not affect the North Sea's primary production in a linear manner. The effects of the NAO, for example, on the North Sea are not the same in every occurrence, which makes prediction difficult. When comparing the primary production results to other literature studies, the results from this project are lower than the ones published. In part, this might have to do with the fact that satellite-derived estimates of chlorophyll-a concentrations do not take into account the presence of a deep chlorophyll maximum. The deep chlorophyll maximum has been shown to contribute up to 30% of the North Sea's NPP values, which may explain why primary production values derived in this project are lower than other studies. Another explanation is that there is no current standard set for the length of the incubation periods used for ^{14}C-GPP measurements. Although GPP measurements are normally performed with 1- or 2-hr incubation periods, studies have shown that even at 2-hour incubation periods, respiration starts to occur, causing the GPP value measured from these 2-hour incubation periods to be underestimated. The lack of an intra-regional standard for length of incubation periods used to measured GPP or NPP respectively makes comparison of values difficult.

Furthermore, the extent of underestimation is not known due to a variety of factors that influences the growth cycle of phytoplankton.

Additionally, it was also found that there have been conflicting results of water clarity and primary production trends for the North Sea, both for modelled and measured values. Due to the non-linear effects of climate change on the environment, and the hydrodynamic heterogeneity of regions in the North Sea, it is still difficult to quantify with high certainty the effects of climate change on North Sea primary production. This project saw a non-significant increasing trend in primary production for the North Sea, but the period of analysis was also too short to investigate long-term trends as it has not satisfied the Nyquist frequency criteria. Furthermore, regime shifts can occur in the North Sea which may result in shifts in phytoplankton dynamics. This is important as different phytoplankton groups have different nutrient requirements or acclimations to the environment, therefore, I have proposed in this project that a future method of assessing overall changes in primary production trends in the North Sea is to separate long-term time series trends by the regime shifts that the North Sea experiences. This may make for better understanding of the dynamic nature of primary production over space and time. It will additionally assist in visualizing how the North Sea reacts to regime shifts, the duration of the regime, and the correlation of such regimes with climatic variability.

In retrospect, the simple primary production model employed in this project has been useful in making good estimates of primary production trends between 2002-2012. It successfully modelled the interannual and intra-regional variability in primary production for the North Sea. This method can therefore be applied to future Sentinel-3 images, provided the algorithms and techniques used in atmospheric correction and parameter retrieval are similar, and can be used to extend the time-series of primary production in the North Sea.

7 References

Aardema, H., Rijkeboer, M., Lefebvre, A., Veen, A. and Kromkamp, J. (2018). High resolution in-situ measurements of phytoplankton photosynthesis and abundance in the Dutch North Sea. *Ocean Science Discussions*, pp.1-37.

Alexeev, V., Walsh, J., Ivanov, V., Semenov, V., Smirnov, A., 2017. Warming in the Nordic Seas, North Atlantic storms and thinning Arctic sea ice. Environmental Research Letters 12, 084011. doi:10.1088/1748-9326/aa7a1d

Ashworth, J., Turkarslan, S., Harris, M., Orellana, M., Baliga, N., 2016. Pan-transcriptomic analysis identifies coordinated and orthologous functional modules in the diatoms Thalassiosira pseudonana and Phaeodactylum tricornutum. Marine Genomics 26, 21-28. doi:10.1016/j.margen.2015.10.011

Balkanski, Y., Monfray, P., Battle, M. and Heimann, M. (1999). Ocean primary production derived from satellite data: An evaluation with atmospheric oxygen measurements. *Global Biogeochemical Cycles*, 13(2), pp.257-271.

Behrenfeld, M. and Falkowski, P., 1997b. Photosynthetic rates derived from satellite-based chlorophyll concentration. Limnology and Oceanography, 42(1), pp.1-20.

Behrenfeld, M. and Falkowski, P., 1997. A consumer's guide to phytoplankton primary productivity models. Limnology and Oceanography, 42(7), pp.1479-1491.

Behrenfeld, M., O'Malley, R., Siegel, D., McClain, C., Sarmiento, J., Feldman, G., Milligan, A., Falkowski, P., Letelier, R., Boss, E., 2006. Climate-driven trends in contemporary ocean productivity. Nature 444, 752-755. doi:10.1038/nature05317

Blanchard, J., Jennings, S., Holmes, R., Harle, J., Merino, G., Allen, J., Holt, J., Dulvy, N., Barange, M., 2012. Potential consequences of climate change for primary production and fish production in large marine ecosystems. Philosophical Transactions of the Royal Society B: Biological Sciences 367, 2979-2989. doi:10.1098/rstb.2012.0231

Brönnimann, S., 2007. Impact of El Niño-Southern Oscillation on European climate. Reviews of Geophysics 45, n/a-n/a. doi:10.1029/2006rg000199

Boitsov, V., Karsakov, A., Trofimov, A., 2012. Atlantic water temperature and climate in the Barents Sea, 2000-2009. ICES Journal of Marine Science 69, 833-840. doi:10.1093/icesjms/fss075

Brockmann Consult, 2014. Consensus Case 2 Regional Algorithm Protocols. CoastColour.

Burson, A., Stomp, M., Akil, L., Brussaard, C., Huisman, J., 2016. Unbalanced reduction of nutrient loads has created an offshore gradient from phosphorus to nitrogen limitation in the North Sea. Limnology and Oceanography 61, 869-888. doi:10.1002/lno.10257

Capuzzo, E., Lynam, C., Barry, J., Stephens, D., Forster, R., Greenwood, N., McQuatters-Gollop, A., Silva, T., van Leeuwen, S., Engelhard, G., 2017. A decline in primary production in the North Sea over 25 years, associated with reductions in zooplankton abundance and fish stock recruitment. Global Change Biology 24, e352-e364. doi:10.1111/gcb.13916

Capuzzo, E., Stephens, D., Silva, T., Barry, J., Forster, R., 2015. Decrease in water clarity of the southern and central North Sea during the 20th century. Global Change Biology 21, 2206-2214. doi:10.1111/gcb.12854

Cole, B., Cloern, J., 1987. An empirical model for estimating phytoplankton productivity in estuaries. Marine Ecology Progress Series 36, 299-305. doi:10.3354/meps036299

Cox, T., Soetaert, K., Vanderborght, J., Kromkamp, J., Meire, P., 2010. Modeling photosynthesis-irradiance curves: Effects of temperature, dissolved silica depletion, and changing community assemblage on community photosynthesis. Limnology and Oceanography: Methods 8, 424-440.

de Kok, J.M., 2002. The influence of fresh water distribution on SPM transport in the Dutch coastal zone. In *Proceedings in Marine Science* (Vol. 5, pp. 563-576). Elsevier.

Deser, C., Hurrell, J., Phillips, A., 2016. The role of the North Atlantic Oscillation in European climate projections. Climate Dynamics 49, 3141-3157. doi:10.1007/s00382-016-3502-z

Desmit, X., Ruddick, K., Lacroix, G., 2015. Salinity predicts the distribution of chlorophyll a spring peak in the southern North Sea continental waters. Journal of Sea Research 103, 59-74. doi:10.1016/j.seares.2015.02.007

Devlin, M., Barry, J., Mills, D., Gowen, R., Foden, J., Sivyer, D. and Tett, P. (2008). Relationships between suspended particulate material, light attenuation and Secchi depth in UK marine waters. *Estuarine, Coastal and Shelf Science*, 79(3), pp.429-439.

Ducrotoy, J. P., Elliott, M., De Jonge, V., 2000. The North Sea. In: Shepard, C. (Ed.), Seas at the Millennium. Elsevier, London.

Ducrotoy, J. P., Elliott, M., 2008. The science and management of the North Sea and the Baltic Sea: Natural history, present threats and future challenges. Marine Pollution Bulletin 57, 8-21. doi:10.1016/j.marpolbul.2008.04.030

Dupont, N., Aksnes, D., 2013. Centennial changes in water clarity of the Baltic Sea and the North Sea. Estuarine, Coastal and Shelf Science 131, 282-289. doi:10.1016/j.ecss.2013.08.010

Eleveld, M.A., van der Woerd, H.J., 2006. Patterns in Water Quality Products of the North Sea: Variogram Analyses of Single and Compound Seawifs Chl & SPM Grids.

European Space Agency (ESA), n.d.. "Sentinel-3 OLCI User Guide". ESA. (https://sentinels.copernicus.eu/web/sentinel/user-guides/sentinel-3-olci). Accessed 25-05-2018.

European Space Agency, 2012. ESA Declares End Of Mission For Envisat.

Falkowski, P., Barber, R., Smetacek, V., 1998. Biogeochemical Controls and Feedbacks on Ocean Primary Production. Science 281, 200-206. doi:10.1126/science.281.5374.200

Fettweis, M., Francken, F., Van den Eynde, D., Verwaest, T., Janssens, J., Van Lancker, V., 2010. Storm influence on SPM concentrations in a coastal turbidity maximum area with high anthropogenic impact (southern North Sea). Continental Shelf Research 30, 1417-1427. doi:10.1016/j.csr.2010.05.001

Flynn, K. (2001). A mechanistic model for describing dynamic multi-nutrient, light, temperature interactions in phytoplankton. *Journal of Plankton Research*, 23(9), pp.977-997.

Friedland, K., Stock, C., Drinkwater, K., Link, J., Leaf, R. Field, C., Behrenfeld, M., Randerson, J., Falkowski, P., 1998. Primary Production of the Biosphere: Integrating Terrestrial and Oceanic Components. Science 281, 237-240. doi:10.1126/science.281.5374.237

Friedland, K., Stock, C., Drinkwater, K., Link, J., Leaf, R., Shank, B., Rose, J., Pilskaln, C., Fogarty, M., 2012. Pathways between Primary Production and Fisheries Yields of Large Marine Ecosystems. PLoS ONE 7, e28945. doi:10.1371/journal.pone.0028945

Friedland, K.D., Record, N.R., Asch, R.G., Kristiansen, T., Saba, V.S., Drinkwater, K.F., Henson, S., Leaf, R.T., Morse, R.E., Johns, D.G. and Large, S.I., 2016. Seasonal phytoplankton blooms in the North Atlantic linked to the overwintering strategies of copepods. *Elem Sci Anth*, *4*.

Gons, H.J., Ebert, J. & Kromkamp, 1997. Optical teledetection of the vertical attenuation coefficient for downward quantum irradiance of photosynthetically available radiation in turbid inland waters. Aquatic Ecology 31: 299. https://doi.org/10.1023/A:1009902627476

Gons, H. (1999). Optical Teledetection of Chlorophyllain Turbid Inland Waters. *Environmental Science & Technology*, 33(7), pp.1127-1132.

Gons, H., Rijkeboer, M., Bagheri, S. and Ruddick, K. (2000). Optical Teledetection of Chlorophyllain Estuarine and Coastal Waters†. *Environmental Science & Technology*, 34(24), pp.5189-5192.

Gwee, R, 2017. Applying a calibrated primary production model to the Scheldt Estuary using Envisat-MERIS images (*Guided research report*). https://goo.gl/G75N7f

Halsey, K., Jones, B., 2015. Phytoplankton Strategies for Photosynthetic Energy Allocation. Annual Review of Marine Science 7, 265-297. doi:10.1146/annurev-marine-010814-015813

Hays, G., Richardson, A., Robinson, C., 2005. Climate change and marine plankton. Trends in Ecology & Evolution 20, 337-344. doi:10.1016/j.tree.2005.03.004

Heip, C., Goosen, N., Herman, P., Kromkamp, J., Middelburg, J., Soetaert, K., 1995. Production and consumption of biological particles in temperate tidal estuaries. Oceanography and Marine Biology: an Annual Review 33, 1-149.

Hirawake, T., Shinmyo, K., Fujiwara, A. and Saitoh, S. (2012). Satellite remote sensing of primary productivity in the Bering and Chukchi Seas using an absorption-based approach. *ICES Journal of Marine Science*, 69(7), pp.1194-1204.

Holt, J., Schrum, C., Cannaby, H., Daewel, U., Allen, I., Artioli, Y., Bopp, L., Butenschon, M., Fach, B., Harle, J., Pushpadas, D., Salihoglu, B., Wakelin, S., 2016. Potential impacts of climate change on the primary production of regional seas: A comparative analysis of five European seas. Progress in Oceanography 140, 91-115. doi:10.1016/j.pocean.2015.11.004

Houde, E., Rutherford, E., 1993. Recent Trends in Estuarine Fisheries: Predictions of Fish Production and Yield. Estuaries 16, 161. doi:10.2307/1352488

Humphreys, M., Achterberg, E., Hopkins, J., Chowdhury, M., Griffiths, A., Hartman, S., Hull, T., Smilenova, A., Wihsgott, J., S. Woodward, E. and Mark Moore, C. (2018). Mechanisms for a nutrient-conserving carbon pump in a seasonally stratified, temperate continental shelf sea. *Progress in Oceanography*.

Hurrell, J., 2001. CLIMATE: The North Atlantic Oscillation. Science 291, 603-605. doi:10.1126/science.1058761

Kimmerer, W., Parker, A., Lidström, U., Carpenter, E., 2012. Short-Term and Interannual Variability in Primary Production in the Low-Salinity Zone of the San Francisco Estuary. Estuaries and Coasts 35, 913-929. doi:10.1007/s12237-012-9482-2

Kirk, J., 2011. Light and photosynthesis in aquatic ecosystems, 3rd ed. Cambridge University Press, Cambridge, UK.

Kraberg, A., Wasmund, N., Vanaverbeke, J., Schiedek, D., Wiltshire, K., Mieszkowska, N., 2011. Regime shifts in the marine environment: The scientific basis and political context. Marine Pollution Bulletin 62, 7-20. doi:10.1016/j.marpolbul.2010.09.010

Kromkamp, J. and Peene, J. (2005). Changes in phytoplankton biomass and primary production between 1991 and 2001 in the Westerschelde estuary (Belgium/The Netherlands). *Hydrobiologia*, 540(1-3), pp. 117-216.

Latasa, M., Cabello, A., Morán, X., Massana, R. and Scharek, R. (2016). Distribution of phytoplankton groups within the deep chlorophyll maximum. *Limnology and Oceanography*, 62(2), pp.665-685.

Laufkötter, C., Vogt, M., Gruber, N., 2013. Long-term trends in ocean plankton production and particle export between 1960–2006. Biogeosciences 10, 7373-7393. doi:10.5194/bg-10-7373-2013

van Leeuwen, S., van der Molen, J., Ruardij, P., Fernand, L., Jickells, T., 2012. Modelling the contribution of deep chlorophyll maxima to annual primary production in the North Sea. Biogeochemistry 113, 137-152. doi:10.1007/s10533-012-9704-5

van Leeuwen, S., Tett, P., Mills, D., & van der Molen, J. (2015). Stratified and non-stratified areas in the North Sea: Long-term variability and biological and policy implications. Journal of Geophysical Research Oceans, 120, 4670–4686. https://doi.org/10.1002/2014jc010485

Lozier, M., Dave, A., Palter, J., Gerber, L., Barber, R., 2011. On the relationship between stratification and primary productivity in the North Atlantic. Geophysical Research Letters 38, n/a-n/a. doi:10.1029/2011gl049414

Lucas, L., Cloern, J., Koseff, J., Monismith, S., Thompson, J., 1998. Does the Sverdrup critical depth model explain bloom dynamics in estuaries?. Journal of Marine Research 56, 375-415. doi:10.1357/002224098321822357

Macedo, M., Duarte, P., Ferreira, J., 2002. The influence of incubation periods on photosynthesis–irradiance curves. Journal of Experimental Marine Biology and Ecology 274, 101-120. doi:10.1016/s0022-0981(02)00202-2

Marasovic, I. and Nincevic, Z., 1997. Primary production - a basic factor in the sea water quality assessment in the middle Adriatic. WIT Transactions on Ecology and the Environment, 20.

McClain, C., 2009. A Decade of Satellite Ocean Color Observations. Annual Review of Marine Science 1, 19-42. doi:10.1146/annurev.marine.010908.163650

McQuatters-Gollop, A., Raitsos, D., Edwards, M., Pradhan, Y., Mee, L., Lavender, S., Attrill, M., 2007. A long-term chlorophyll dataset reveals regime shift in North Sea phytoplankton biomass unconnected to nutrient levels. Limnology and Oceanography 52, 635-648. doi:10.4319/lo.2007.52.2.0635

Milligan, A., Halsey, K., Behrenfeld, M., 2015. Advancing interpretations of14C-uptake measurements in the context of phytoplankton physiology and ecology: Fig. 1. Journal of Plankton Research 37, 692-698. doi:10.1093/plankt/fbv051

Ministry of Infrastructure and the Environment & Ministry of Economic Affairs, 2015. The Policy Document on the North Sea 2016-2021. The Hague.

Moll, A., 1997. Modeling Primary Production in the North Sea. Oceanography 10, 24-26. doi:10.5670/oceanog.1997.41

Moore, J., Fu, W., Primeau, F., Britten, G., Lindsay, K., Long, M., Doney, S., Mahowald, N., Hoffman, F., Randerson, J., 2018. Sustained climate warming drives declining marine biological productivity. Science 359, 1139-1143. doi:10.1126/science.aao6379

Morel, A., Smith, R., 1974. Relation between total quanta and total energy for aquatic photosynthesis. Limnology and Oceanography 19, 591-600. doi:10.4319/lo.1974.19.4.0591

Morris, E., Kromkamp, J., 2003. Influence of temperature on the relationship between oxygen- and fluorescence-based estimates of photosynthetic parameters in a marine benthic diatom (Cylindrotheca closterium). European Journal of Phycology 38, 133-142.

National Space Science Data Center (n.d.). "Coastal Zone Color Scanner". NASA. (https://nssdc.gsfc.nasa.gov/nmc/experimentDisplay.do?id=1978-098A-03) Accessed: 13-05-2018

Nienhuis, P., Smaal, A., 1994. The Oosterschelde estuary, a case-study of a changing ecosystem: an introduction. Hydrobiologia 282-283, 1-14. doi:10.1007/bf00024616

Paramor, O., Allen, K., Aanesen, M., Armstrong, C., Hegland, T., Le Quesne, W., Piet, G., Raakær, J., Rogers, S., van Hal, R., van Hoof, L., van Overzee, H., Frid C., 2009. MEFEPO North Sea Atlas. University of Liverpool. ISBN 0 906370 60 4

Paul, J.H. and Pichard, S.L., 1998. Phytoplankton activity through the measurement of ribulose bisphosphate carboxylase gene expression (Rubisco). Molecular Approaches to the Study of the Ocean, 207-225. Springer, Dordrecht.

Pauly, D., Christensen, V., 1995. Primary production required to sustain global fisheries. Nature 374, 255-257. doi:10.1038/374255a0

Pemberton, K., Clarke, K., Joint, I., 2006. Quantifying uncertainties associated with the measurement of primary production. Marine Ecology Progress Series 322, 51-59. doi:10.3354/meps322051

Pikitch, E., Santora, C., Babcock, E.A., Bakun, A., Bonfil, R., Conover, D.O., Dayton, P.A.O., Doukakis, P., Fluharty, D., Heneman, B. and Houde, E.D., 2004. Ecosystem-based fishery management. Science, 305(5682), pp.346-347.

Ruddick, K., Lacroix, G., Lancelot, C., Nechad, B., Park, Y., Peters, S., Van Mol, B., 2008. Optical Remote Sensing of the North Sea. Remote Sensing of the European Seas 79-90. doi:10.1007/978-1-4020-6772-3_6

Sarmiento, J., Slater, R., Barber, R., Bopp, L., Doney, S., Hirst, A., Kleypas, J., Matear, R., Mikolajewicz, U., Monfray, P., Soldatov, V., Spall, S., Stouffer, R., 2004. Response of ocean ecosystems to climate warming. Global Biogeochemical Cycles 18, n/a-n/a. doi:10.1029/2003gb002134

STECF, 2016. The 2016 Annual Economic Report on the EU Fishing Fleet. Publications Office of the European Union, Luxembourg.

Tagliabue, A., Bopp, L. and Gehlen, M. (2011). The response of marine carbon and nutrient cycles to ocean acidification: Large uncertainties related to

phytoplankton physiological assumptions. *Global Biogeochemical Cycles*, 25(3), p.n/a-n/a.

Thomas, H., Bozec, Y., de Baar, H., Elkalay, K., Frankignoulle, M., Schiettecatte, L., Kattner, G., Borges, A., 2005. The carbon budget of the North Sea. Biogeosciences 2, 87-96. doi:10.5194/bg-2-87-2005

Tilstone, G., Taylor, B., Blondeau-Patissier, D., Powell, T., Groom, S., Rees, A. and Lucas, M. (2015). Comparison of new and primary production models using SeaWiFS data in contrasting hydrographic zones of the northern North Atlantic. *Remote Sensing of Environment*, 156, pp.473-489.

Tiselius, P., Belgrano, A., Andersson, L., Lindahl, O., 2015. Primary productivity in a coastal ecosystem: a trophic perspective on a long-term time series. Journal of Plankton Research 38, 1092-1102. doi:10.1093/plankt/fbv094

Van Der Woerd, H. and Pasterkamp, R. (2008). HYDROPT: A fast and flexible method to retrieve chlorophyll-a from multispectral satellite observations of optically complex coastal waters. *Remote Sensing of Environment*, 112(4), pp.1795-1807.

Varela, R., Cruzado, A., Gabaldón, J., 1995. Modelling primary production in the North Sea using the European Regional Seas Ecosystem Model. Netherlands Journal of Sea Research 33, 337-361. doi:10.1016/0077-7579(95)90052-7

Vermaat, J., McQuatters-Gollop, A., Eleveld, M., Gilbert, A., 2008. Past, present and future nutrient loads of the North Sea: Causes and consequences. Estuarine, Coastal and Shelf Science 80, 53-59. doi:10.1016/j.ecss.2008.07.005

de Vries, I., Duin, R., Peeters, J., Los, F., Bokhorst, M., Laane, R., 1998. Patterns and trends in nutrients and phytoplankton in Dutch coastal waters: comparison of time-series analysis, ecological model simulation, and mesocosm experiments. ICES Journal of Marine Science 55, 620-634. doi:10.1006/jmsc.1998.0399

Walczowski, W., Piechura, J., Goszczko, I., Wieczorek, P., 2012. Changes in Atlantic water properties: an important factor in the European Arctic marine climate. ICES Journal of Marine Science 69, 864-869. doi:10.1093/icesjms/fss068

Walker, A. N., Keller, K., Pieters, A. J., 2016. Economic description of the Dutch North Sea and Coast: 2005, 2010, 2014. Statistics Netherlands, The Hague.

Weijerman, M., Lindeboom, H., Zuur, A., 2005. Regime shifts in marine ecosystems of the North Sea and Wadden Sea. Marine Ecology Progress Series 298, 21-39. doi:10.3354/meps298021

Weston, K., Fernand, L., Mills, D., Delahunty, R., Brown, J., 2005. Primary production in the deep chlorophyll maximum of the central North Sea. Journal of Plankton Research 27, 909-922. doi:10.1093/plankt/fbi064

8 Appendix
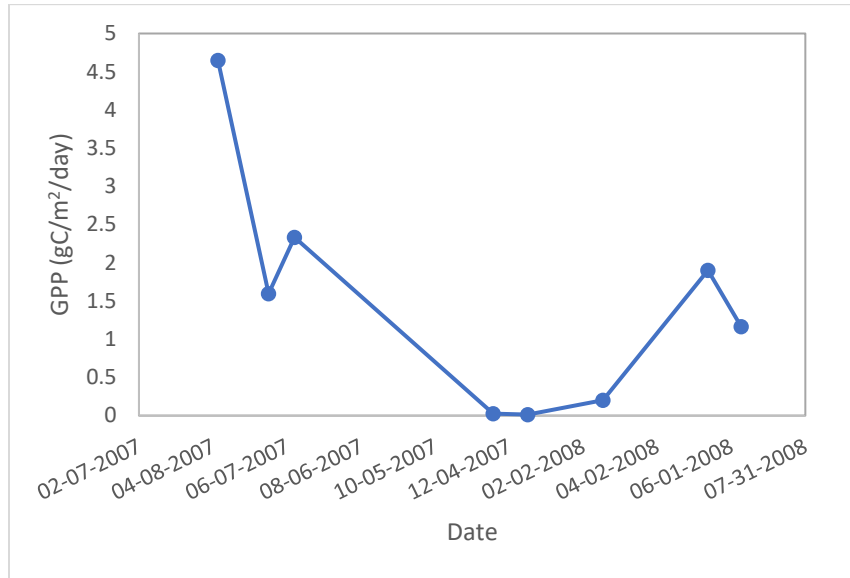
*Supplementary 1: ^{14}C-based GPP measurements over 2-hr incubation periods for OS9. Total of 8 sample points over 2 years spanning different seasons.*
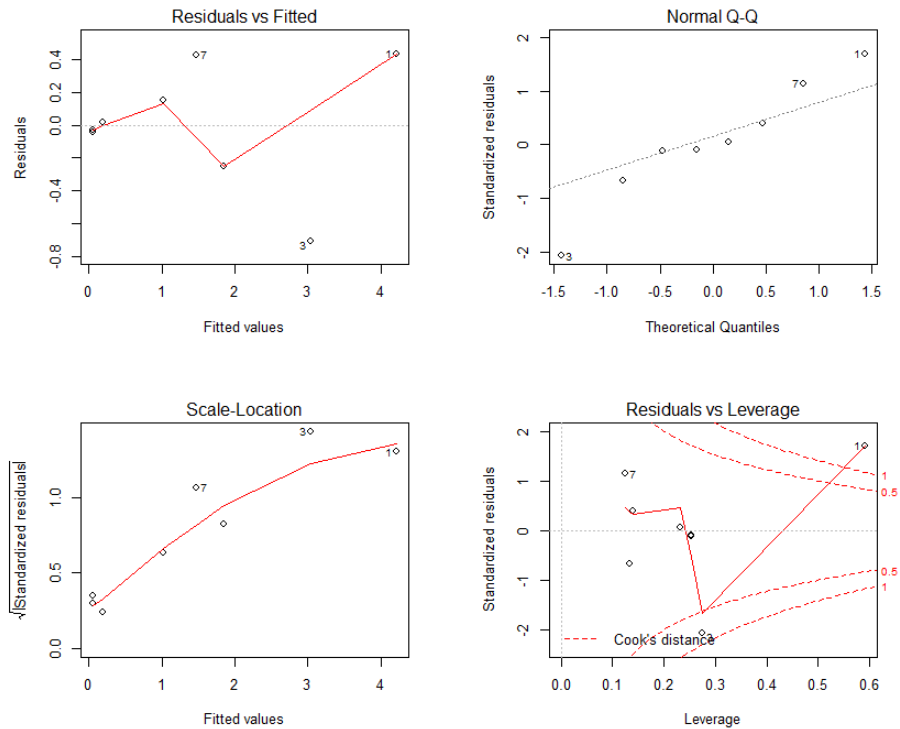
Supplementary 2: Results of ANOVA performed on GPP versus the BPI composite values in OS9

	Degree of freedom	Sum Square	Mean Square	F value	Pr(>F)
BPI composite	1	15.998	15.998	100.3	5.74e-05 ***
Residuals	6	0.957	0.159		
Significant codes:	0 '***' 0.001 '**' 0.01 '*' 0.05 '.' 0.1 ' ' 1				

Supplementary 3: Table of ANOVA test results, with p-values smaller than 0.001 showing significant relationship between datasets
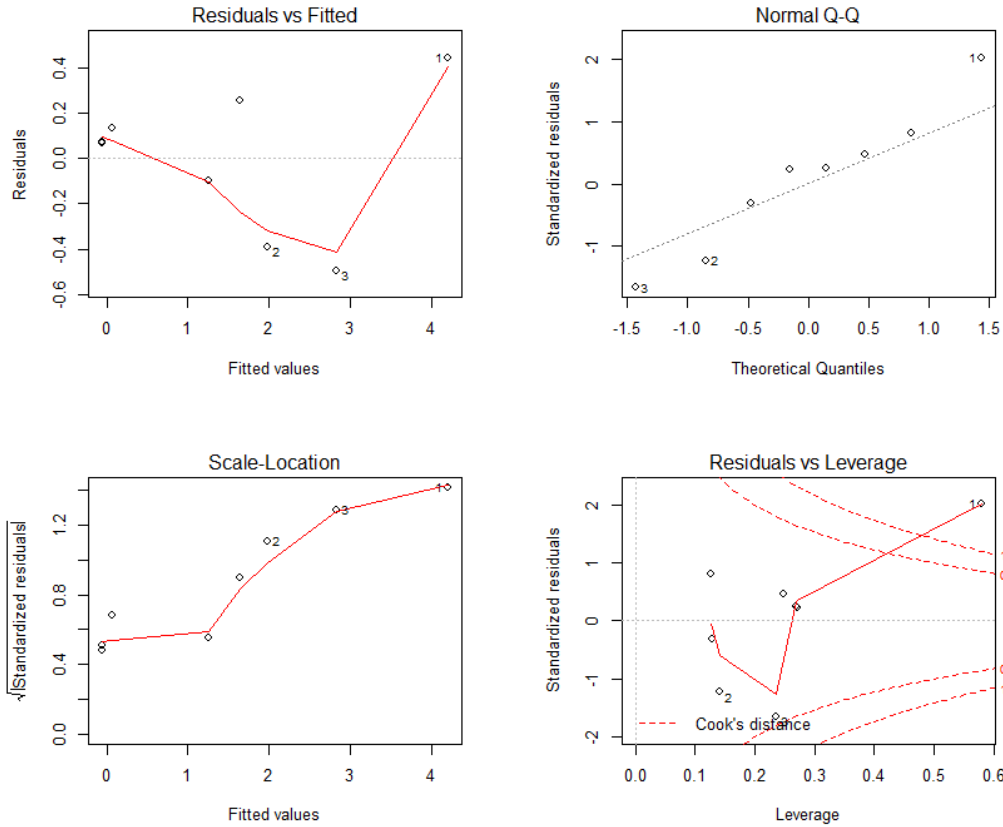
Supplementary 4: ANOVA performed on GPP values versis BPI*P^b_{max} values
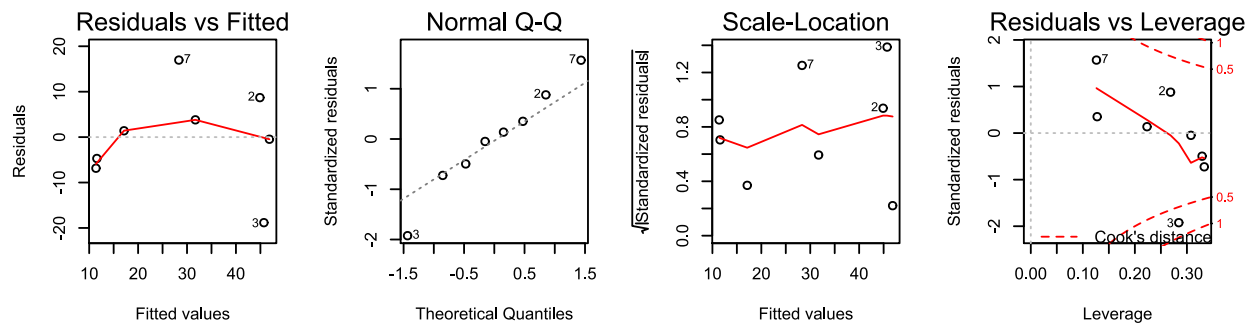
Supplementary 5: ANOVA performed on measured versus modelled E_o values

Residuals:

Min	1Q	Median	3Q	Max
-29.939	-1.704	-1.004	0.909	37.040

Coefficients:

	Estimate	Std. Error	t value	Pr(>|t|)
Intercept	1.927771	0.27983	6.889	$1.68 * 10^{-11}$
Satellite	0.46863	0.02025	23.137	$< 2 * 10^{-16}$
Significant codes:	0 '***' 0.001 '**' 0.01 '*' 0.05 '.' 0.1 ' ' 1			

Residual standard error: 5.582 on 506 degrees of freedom
Multiple R-squared: 0.5141,   Adjusted R-squared: 0.5131
F-statistic: 535.3 on 1 and 506 DF, p-value: < 2.2e-16

Supplementary 6: Linear regression analysis statistical summary for North Sea chlorophyll-a (measured versus satellite)

Residuals:

Min	1Q	Median	3Q	Max
-0.79555	-0.09370	-0.01666	0.10396	0.91033

Coefficients:

	Estimate	Std. Error	t value	Pr(>|t|)
Intercept	0.09205	0.04366	2.108	0.0405
Satellite	1.56300	0.13310	11.743	$1.93 * 10^{-15}$
Significant codes:	0 '***' 0.001 '**' 0.01 '*' 0.05 '.' 0.1 ' ' 1			

Residual standard error: 0.2226 on 46 degrees of freedom
Multiple R-squared: 0.7499,   Adjusted R-squared: 0.7444
F-statistic: 137.9 on 1 and 46 DF, p-value: 1.929e-15

Supplementary 7: Linear regression analysis summary for measured versus satellite values of light attenuation coefficient (K_d) in the North Sea

Residuals:

Min	1Q	Median	3Q	Max
-64.313	-3.362	-2.365	-0.172	83.83

Coefficients:

	Estimate	Std. Error	t value	Pr(>|t|)
Intercept	4.83213	0.70057	6.897	4.7e-11 ***
Satellite	0.96129	0.06259	15.358	<2e-16 ***
Significant codes:	0 '***' 0.001 '**' 0.01 '*' 0.05 '.' 0.1 ' ' 1			

Residual standard error: 10.23 on 239 degrees of freedom
Multiple R-squared: 0.4967,   Adjusted R-squared: 0.4946
F-statistic: 235.9 on 1 and 239 DF, p-value: < 2.2e-16

Supplementary 8: Linear regression analysis summary for measured versus satellite values of SPM in the North Sea
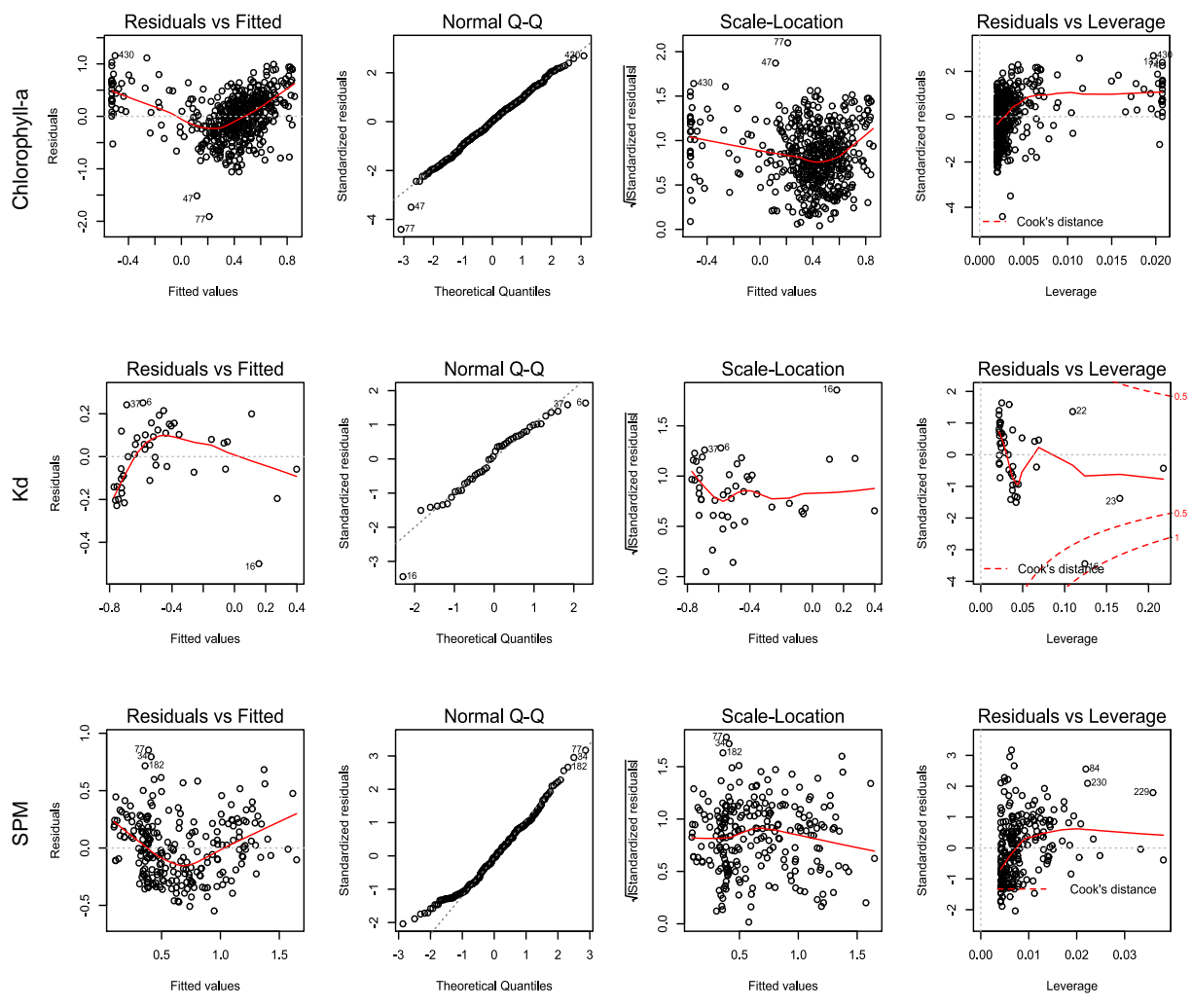
Supplementary 9: ANOVA analysis of log$_{10}$-transformed measured versus satellite-derived water quality parameters

Date	E_o	GPP	LogGPP	Chl-a	Kd	P^b_{max}	Temp. (°C)	SPM	BPI	Modelled GPP	BPI*Pmax	logBPI	Log(BPI*P$_{max}$)	Model	R^2
12-04-2007	35.51209	4.649	0.667359546	22.007	0.622	5.692988	10.7	6.01	5779.69	4.213243132	32903.7	3.761905	4.517245	BPI	0.943562
*23-05-2007	53.59249	1.598	0.203576775	3.672	0.362	6.320661	14.9	5.04	2500.667	1.849067916	15805.87	3.398056	4.198818	BPI*P_{max}	0.95862
13-06-2007	26.87886	2.333	0.367914739	10.938	0.326	5.375183	16.2	6.311111	4148.48	3.037140867	22298.84	3.617889	4.348282	logBPI	0.989876
21-11-2007	4.534295	0.025	-1.602059991	1.017	1.55	5.21591	9.9	26.14444	13.68538	0.055954158	71.3817	1.136257	1.853587	logBPI*P_{max}	0.993809
*19-12-2007	6.8636	0.014	-1.853871964	1.457	3.287	3.693939	6.0	49.56	13.99489	0.056177319	51.69629	1.14597	1.713459		
*18-02-2008	18.51257	0.204	-0.690369833	1.65	0.735	5.10305	6.6	11.75333	191.1706	0.183921028	975.5533	2.281421	2.989251		
*13-05-2008	45.28941	1.9	0.278753601	6.516	0.686	6.643056		2.085714	1978.844	1.472833211	13145.57	3.296411	4.118779		
09-06-2008	46.37597	1.163	0.065579715	3.815	0.607	7.60172		6.01	1340.777	1.012787505	10192.21	3.127357	4.008269		

Supplementary 10: In-situ measured water quality parameters from station OS9. The table also includes the calculated BPI values and the respective modelled GPP values.
Dates that coincided with MERIS image availability.

Longitude	Latitude
2.978268	52.407909
2.978268	52.757909
2.978268	53.107909
2.978268	53.457909
2.978268	53.807909
2.978268	54.157909
2.978268	54.507909
2.978268	54.857909
2.978268	55.207909
2.978268	55.557909
2.978268	55.907909
2.978268	56.257909
2.978268	56.607909
2.978268	56.957909
2.978268	57.307909
2.978268	57.657909
2.978268	58.007909
2.978268	58.357909
2.978268	58.707909
2.978268	59.057909

Supplementary 11: Coordinates of the North-South transect used for generating latitudinal variations in primary production